

國立臺灣大學電機資訊學院生醫電子與資訊學研究所

碩士論文

Graduate Institute of Biomedical Electronics and Bioinformatics

College of Electrical Engineering and Computer Science

National Taiwan University

Master Thesis

以微分方程系統解析粒線體對細胞核傳訊的系統特性

Understanding the System Dynamics of
Mitochondrial Retrograde Signaling from a Differential
Equation-based Framework

邱紹庭

Shao-Ting Chiu

指導教授：魏安祺 博士

Advisor: An-Chi Wei Ph.D.

中華民國 110 年 8 月

August, 2021

國立臺灣大學碩士學位論文

口試委員會審定書

以微分方程系統解析粒線體對細胞核傳訊的系統
特性

Understanding the System Dynamics of
Mitochondrial Retrograde Signaling from a
Differential Equation-based Framework

本論文係邱紹庭君 (R07945001) 在國立臺灣大學生醫電
子與資訊學研究所完成之碩士學位論文，於民國 109 年 1 月 28 日
承下列考試委員審查通過及口試及格，特此證明

口試委員：

賴安祺

(指導教授)

江介宏

黃乙

阮雪芬

張瑞峰

所長：

張瑞峰





Acknowledgements

I would like to express my sincere gratitude to my supervisor Dr. An-Chi Wei for the continuous support throughout this research. Her guidance and inspiration were invaluable. In addition, I would like to thank my thesis committee: Dr. Hsueh-Fen Juan, Dr. Hsuang-Cheng Huang, Dr. Jie-Hong Jiang and Dr. Jun-Yi Leu, for insightful comments and suggestions.

Special thanks to Dr. Brian O'Rourke, for offering me the summer internship at Johns Hopkins University. His guidance on the field of cardiac mitochondria was inspiring.

Besides, thanks to my fellow labmates in Biological Systems Group. Chan-Min Hsu for working together on the deep learning of image classification and ICSB2019; Yu-De Lin for the stimulating discussions about both my research and career; Also, Yu-Zhi Chen, J.C. Huang, Chin-Hsian Zhu, Yi-Ju Lee, and many others who joined my presentation during the meeting and accompanied me throughout this project.

In particular, my sincere thanks go to Wen-Wei Tseng for his patient guidance on modeling and simulation. His introduction to Julia programming language has brought me to state-of-art scientific computing, opening a gate to many opportunities.

Finally, I would like to thank my family for their enormous patience and love. Without them, this journey would not have been successful. I dedicate this milestone to them.





摘要

粒線體是一種存在於真核細胞中的半自主性胞器，擔任細胞的能量工廠和代謝樞紐，其功能仰賴於細胞核基因體的供給與維護。因此粒線體對細胞核的傳訊過程在修補粒線體上扮演重要的角色。文獻上的研究著重於傳訊過程參與的蛋白質種類，與在不同狀態下對於基因體的定性調控。然而對於此粒線體網路的通訊性質仍所知甚少。本篇論文採取控制系統的角度，以酵母菌為模式生物，整合粒線體往細胞核傳訊的分子機制，其中包含蛋白質結合與轉錄因子進入細胞核的過程。透過酵素動力學理論，以常微分方程系統來探討粒線體訊號傳遞的過程。本論文分成三個部分，第一部分為粒線體傳訊的布林模型；第二部分為常微分模型；第三部分為隨機系統模型。模擬出蛋白分子濃度在粒線體損害的動態過程包含波型、頻率響應及在雜訊影響下的可靠性。進一步的模擬與演算顯示，粒線體傳訊網路為近似於一個雙穩態系統，並附加三個區域性的穩態點。此外，訊號蛋白競爭型結合的過程，是提升敏感度的機制。透過隨機模擬亦發現訊號噪訊比會隨著粒線體損傷訊號增強而減少。本論文提出了粒線體傳訊的數學模型，以定量的角度思考資訊傳遞的過程。這不僅能夠更了解粒線體往細胞核傳訊的機制，也可能應用於致病性酵母的藥物研發與投藥策略。

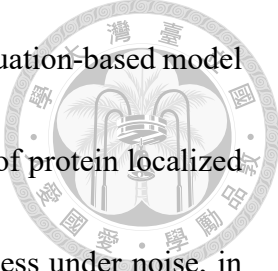
關鍵字：粒線體逆向訊號、酵素動力學、數學模型、控制系統、常微分方程





Abstract

The mitochondrion is a semi-autonomous organelle in eukaryotic cells and participates in the energy production and versatile metabolic regulations. These roles make mitochondrial quality control essential to maintain its functionality. While most mitochondrial genes are located in the nucleus genome, the quality control depends on supplements from the nucleus. The mitochondrial retrograde signaling describes the communication between mitochondria and the nucleus, which plays a critical role in regulating the nucleus genome. Published studies have focused on the signaling pathway participants and the qualitative effect of knockouts on genome expressions. However, there is a lack of understanding of this pathway's communication characteristics, and how mitochondrial signal is modulated throughout the process remains unclear. To simulate the signal propagation from the mitochondrial damage, we use yeast as a model organism and propose a novel mathematical model of mitochondrial retrograde signaling based on enzyme kinetics and ordinary differential equations (ODE). This study contains three parts: (1) A



boolean model of mitochondrial signaling (2) Ordinary differential Equation-based model
(3) Extended stochastic model. The simulation reveals the dynamics of protein localized concentration including waveforms, frequency response, and robustness under noise, in response to mitochondrial damage. Further analysis shows that the mitochondrial retrograde signaling is a bistable system with three localized steady states and the competitive binding results in the ultrasensitivity. By applying stochastic simulation, we found that the increased mitochondrial damage signal can deteriorate the robustness. This study unravels the quantitative mechanism of mitochondrial retrograde signaling and may provide drug design applications for pathogenic yeast and antifungal therapy.

Keywords: Mitochondrial retrograde signaling (RTG), enzyme kinetics, mathematical modeling, control systems, ordinary differential equations



Contents

	Page
Verification Letter from the Oral Examination Committee	i
Acknowledgements	iii
摘要	v
Abstract	vii
Contents	ix
List of Figures	xiii
List of Tables	xv
Denotation	xvii
Chapter 1 Introduction	1
1.1 Mitochondria quality control- An overview	1
1.2 Mitochondrial retrograde signaling in yeast	2
1.3 Mitochondrial signaling as a communication system	3
1.4 An ordinary differential equation-based model for mitochondrial retrograde signaling	4
1.5 Application of this Study	5
Chapter 2 Methods and Materials	7
2.1 The structure of the differential equation-based model of mitochondrial retrograde signalling in yeast	7

2.2	A Boolean model of mitochondrial network	8
2.3	The expression levels of RTG genes	10
2.4	From Boolean model to ordinary differential equation-based model	11
2.5	Parameter searching with the qualitative data of protein translocation	14
2.6	An ordinary differential equation-based model of mitochondrial retrograde signaling in yeast	17
2.7	Ultrasensitivity analysis with relative amplification approach	19
Chapter 3	Results	23
3.1	The steady states of 18 mitochondrial-related conditions are verified by the qualitative studies.	23
3.2	The ultrasensitivity of Bmh/Mksp degradation causes the switch-like response of Rtg1/3p to mitochondrial damage	25
3.3	The competitive binding between Bmhp and Rtg2p with Mksp contributes to the ultrasensitivity of Bmh/Mksp degradation	27
3.4	Quantitative analysis of the activation layer	30
3.4.1	The analytical solution of the activation layer	30
3.4.2	The competitive binding of Bmhp and Rtg2p with Mksp is the source of the ultrasensitivity.	31
3.5	Frequency modulation of mitochondrial retrograde signaling	34
3.6	Robustness analysis	38
Chapter 4	Discussion	41
Chapter 5	Concluding Remarks	45
5.0.1	Significance of this study	45
5.0.2	Limitation	46

5.0.3	Future perspective	47
References		49
Appendix A — Key Resources		63
Appendix B — Boolean model of mitochondrial retrograde signaling		65
B.0.4	Stress response and expression levels	65
B.0.5	Model with dynamical inputs	67
B.0.6	Rtg1/3p Translocation under Multiple Conditions	72
B.0.7	Ordinary differential equation-based model of mitochondrial retro- grade signaling	74
B.0.8	Fitted parameters	76
Appendix C — Package development		81
C.0.9	<i>FindSteadyStates.jl</i> - A Julia package for searching steady states of ODE systems	83



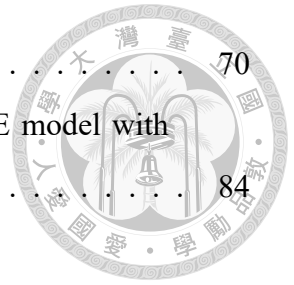




List of Figures

Figure 1.1	The workflow of the experimental design	6
Figure 2.1	Boolean equivalent circuit of Rtg1/3p translocation.	10
Figure 2.2	The circuit of mitochondrial-to-nucleus communication	19
Figure 3.1	Boolean decision in RTG signaling pathway	24
Figure 3.2	Step responses of Bmh/Mksp, Rtg1p _n and Rtg3p _n	26
Figure 3.3	Ultrasensitivity of Bmh/Mksp heterodimer results from molecular titration.	29
Figure 3.4	The frequency response of mitochondrial damage signal and RTG protein concentrations	36
Figure 3.5	The frequency analysis of Bmh/Mksp, Rtg1p _n and Rtg3p _n in respect of mitochondrial damage	37
Figure 3.6	Potential map of the Rtg1/3p translocation in response to mitochondrial damage signal.	39
Figure 4.1	Mitochondrial retrograde circuit	44
Figure B.1	Expression levels of RTG proteins	66
Figure B.2	Pseudo time plots of yeast gene expression	66
Figure B.3	The retrograde response to mitochondrial damage with sigmoid.	67
Figure B.3	The retrograde response to mitochondrial damage with square and sinusoidal waveforms.	68
Figure B.4	The input-output relation and Hill coefficient	69
Figure B.5	The square wave response of the proposed mitochondrial retrograde signalling model	69

Figure B.6 The steady-state of Mksp and its heterodimers	70
Figure C.7 Sample code for exploring steady states of an ODE model with <i>FindSteadyStates.jl</i>	84





List of Tables

Table 2.1	The expression levels of RTG proteins from the quantitative Western blot	11
Table A.1	Key Resources	64
Table B.2	RTG-associated proteins	71
Table B.4	The Boolean model of mitochondrial retrograde signaling	73
Table B.5	Properties of Rtg1/3p translocation to nucleus	73
Table B.6	Parameter set of the proposed model	79





Denotation

RTG	Retrograde Signaling
$\Delta\Phi_m$	Mitochondrial membrane potential
ODE	Ordinary differential equation



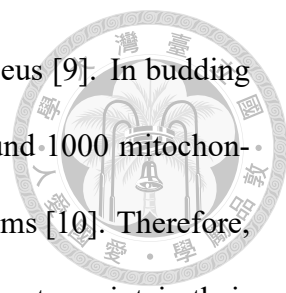


Chapter 1 Introduction

1.1 Mitochondria quality control- An overview

Mitochondria serve as the cells' powerhouse. They utilize the established proton motive force to generate the high-energy molecule ATP to perform cellular work [1]. The analogy of a simple electrical circuit model is an easy way to facilitate understanding of the interactions between ion dynamics and energetics in the complex mitochondrial system [2]. Mitochondria play multiple roles in regulating cellular physiological and pathological mechanisms, including the generation of ATP, the regulation of signaling transduction, immune response, and cell apoptosis [1]. Therefore, mitochondria also serve as an essential cellular regulator, metabolic hub, pathway trigger, and signal hub [3].

However, their versatile roles make them prone to be damaged [4, 5]. Mitochondrial quality control is essential to cell viability due to their participation in hundreds of biochemical reactions from energy production [1], lipid synthesis [6] and reactions of amino acids [7]. These versatile functions require elaborate quality control to maintain mitochondrial functionality, but retrieving energy via electron transport chain makes mitochondria themselves prone to be damaged by oxidative stress [8]. Unlike other membrane-bounded organelle rely solely on the products from nucleus genome, mitochondria possess their own genome, enzymes and repairing systems, but they are actually semi-autonomous or-



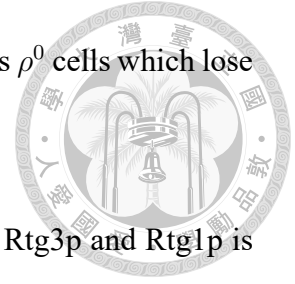
ganelle because most of mitochondrial genes are translocated in nucleus [9]. In budding yeast, only 35 genes are located in mitochondrial matrix out of around 1000 mitochondrial proteins, which are a small fraction of the whole metabolic systems [10]. Therefore, mitochondria require products from genes encoded in nucleus genome to maintain their functionality. The interaction between mitochondria and nucleus genome is a two-way process [3, 11]. Once mitochondria are damaged, their statuses will report to nucleus by sending molecular signals or interfering with metabolic system, and then enabling a cell to coordinate mitochondrial biogenesis. Therefore, mitochondrial quality control depends on the feedback of mitochondrial network status, which is known as mitochondrial retrograde signaling [12, 5, 11, 13].

1.2 Mitochondrial retrograde signaling in yeast

The most detailed mitochondrial retrograde signaling is the RTG pathway discovered in budding yeast [14, 15, 16, 17, 11]. The retrograde signaling is turned on when mitochondria is compromised [18]. These perturbation results in the rearrangement of carbohydrate and nitrogen metabolism [19]. One of regulated genes is *CIT2*, which encodes a peroxisomal isoform of citrate synthase that involves in the glyoxylate cycle, and bypasses the steps in TCA cycle. Thus, the up-regulation of *CIT2* enables a more efficient usage of carbon sources when mitochondria are damaged.

The mechanism of protein interaction has been discovered by using yeast deletion strains. In [14], RTG genes were knocked out separately, and used green fluorescent protein (GFP) to localize RTG proteins. Their results reveal the localization of RTG proteins under different conditions. They compared the localization of RTG proteins under dele-

tion strains, and using strains with dysfunctional mitochondria, such as ρ^0 cells which lose the entire mitochondrial genome in mitochondrial matrix.



Without Rtg2p sensing mitochondrial status, the localization of Rtg3p and Rtg1p is independent of the mitochondrial damage due to the constant inhibition from Bmh/Mksp heterodimer [14], and both Rtg3p and Rtg1p remain cytoplasmic when mitochondria are dysfunctional (ρ^0 strain) [14]. In addition, Rtg1p regulates the translocation of Rtg3p. Though this regulation participates in the activation of the retrograde signaling, the presence of Rtg1p keeps Rtg3p cytoplasmic when mitochondria are undamaged. Besides, without Rtg1p, Rtg3p translocates to the nucleus, and this relocation is independent of the mitochondrial damage.

Though Rtg3p partakes in the activation of retrograde response, the initiation of retrograde response requires nucleus accumulation of both Rtg3p and Rtg1p. Besides, They are both basic helix-loop-helix (bHLH) transcription factors that regulate the retrograde response genes like an AND gate [20, 14, 21]. On the other hand, Rtg1p is both a positive regulator of retrograde response genes transcription, and a negative regulator which keeps Rtg3p cytoplasmic when mitochondrial damage signal is off.

1.3 Mitochondrial signaling as a communication system

However, a cell usually contains multiple mitochondria, and each of them shares the same signaling pathway. The messenger proteins collect the signal from individual mitochondria, and the information is merged in the downstream, causing a multiplexing problem which is first described in telecommunications [22]. One of the famous examples about multiplexing is the Cocktail Party Problem [23] which describes how to selec-

tively decode the information from a particular stimuli when the signal is merged with multiple sources. In the field of engineering, this problem can be solved by independent components analysis (ICA) which can extract individual component from a mixture of non-Gaussian signals [24]. While how eukaryotic cells decode the merged mitochondrial signal is yet to be discussed.

Besides, the noise of the biochemical pathway restricts the ability of a cell to gather information from its organelle. The heat and stochastic nature of chemical reaction are detrimental to the communication between mitochondria and the nucleus. The current studies about retrograde signaling are limited to the protein interactions, differential expressions and their effect on genomic regulation based on the qualitative approach.

To my knowledge, no existing model is describing the noise modulation of the mitochondrial retrograde pathway, and the effect of protein concentration on the noise propagation. In eukaryotic cells like budding yeast, their mitochondria interact with one nucleus via the same biochemical channel, the multiplexing problem and noise are barriers for nucleus genome to access messages from a mitochondrion. It is still unclear how biological systems manage this multiplexing network between mitochondria and the nucleus.

1.4 An ordinary differential equation-based model for mitochondrial retrograde signaling

To investigate the communication properties of mitochondrial retrograde signaling, we developed a differential equation-based model to simulate the process. The mathematical modeling describes how variables change along with time. This dynamics is illustrated

by ordinary differential equations (Eq. 1.1).

$$\frac{d\vec{P}r_{RTG}}{dt} = f(D_{MT}(t), \vec{P}r_{RTG}) \quad (1.1)$$

where $\vec{P}r_{RTG}$ denotes concentrations of RTG-associated proteins, and $D_{MT}(t)$ is the mitochondrial damage at time t .

The mitochondrial status and deleted genes are defined as input and the translocation of Rtg1p/Rtg3p as output. Those relations are observed by microscopy in [14], and summarized in a boolean table. The parameters are fitted with the boolean relation by Monte Carlo Simulation. A parameter set can be verified by solving the steady-states under each observed genotype. Our novel mathematical model can interpret the dynamics of mitochondrial retrograde signaling.

1.5 Application of this Study

The molecular mechanism of retrograde response facilitates the adaptation of eukaryotic organism to unfavorable factors [25, 26]. In yeast, the key role of retrograde signaling pathway is to regulate mitochondrial functional state and metabolic reprogramming including maintenance of intracellular glutamate supplies [27, 25]. Recently, several studies have found an association between retrograde response and drug resistance in yeast [28, 25, 29]. For example, Rtg3p is essential for the antifungal drug tolerance associated with the formation of fungal plasma membrane which consists of ergosterol [30]. Also, $\Delta rtg3$ mutant of pathogenic yeast, *Candida albicans*, displayed declined biofilm formation and adherence to epithelial cell, resulting in reduced infectivity in *C. elegans* [29].



In *S. cerevisiae*, the pleiotropic drug resistance (PDR) is activated by retrograde signaling and induces the transcription of PDR genes [25]. Furthermore, the retrograde signaling is associated with aging, making yeast as a model organism to study mitochondrial quality control and its influences on lifespan [31]. In our study, we proposed a mathematical model to illuminate the communication characteristics of mitochondrial retrograde signaling, and have potential application on research of antifungal drugs and aging.

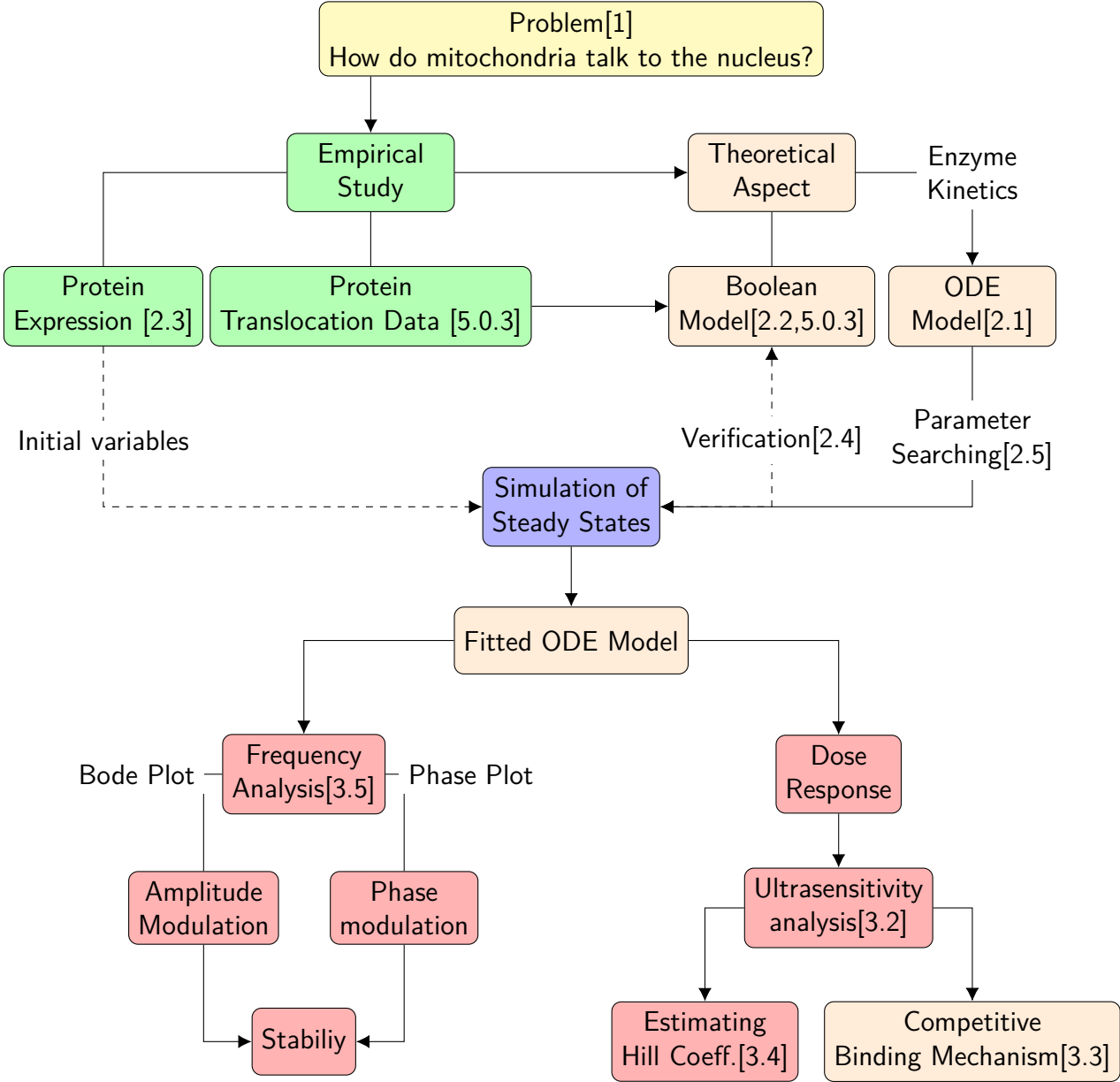


Figure 1.1. The workflow of the experiment design.



Chapter 2 Methods and Materials

2.1 The structure of the differential equation-based model of mitochondrial retrograde signalling in yeast

Mitochondrial retrograde signalling is the communication between the mitochondrial network and the nucleus, which is essential for mitochondrial quality control. In our study, we focus on the RTG pathway in yeast, especially *Saccharomyces cerevisiae*. To understand the mechanism of RTG signalling, we summarize the results of [14], [27] and [31], and derived the mathematical model based on differential equations.

To begin with, Rtg2p is a sensor of mitochondrial damage signal. Though detailed mechanism is unclear, it is hypothesized that the activation of Rtg2p is induced by the loss of mitochondrial membrane potential [8]. Another research reveals that the ATP-binding site of Rtg2p makes its activation a possible indicator of the low ATP/ADP ratio, which is related to the insufficient energy production when mitochondria are dysfunctional.

Bmhp is an inhibitor of the RTG pathway. However, solely existence of Bmhp without binding with Mksp is unable to depress the downstream. When mitochondria are functional, the heterodimer of Bmhp and Mksp is a bottleneck inhibitor which constantly shuts off RTG pathway by keeping Rtg3p, a transcription factor with nuclear localization

sequence (NLS), hyperphosphorylated and staying cytoplasmic.

The activation of RTG pathway starts from the competitive binding between Bmhp and activated Rtg2p. The activation of Rtg2p results from the mitochondrial damage which causes the loss of membrane potential or decreased ATP/ADP ratio. The activated Rtg2p can bind to Mksp, and decrease the abundance of Bmh/Mksp heterodimer. As mentioned below, the Bmh/Mksp is the main inhibitor of the RTG pathway, so the annihilation of it results in the unphosphorylation and also the nucleus accumulation of Rtg3p.

The activation of RTG genes requires the nucleus accumulation of both Rtg3p and Rtg1p. Unlike Rtg3p, there is no NLS found in the structure of Rtg1p, its nucleus accumulation is contributed by its binding with Rtg3p. The dual regulation of Rtg1p on the nucleus accumulation of Rtg3p were first discovered by [14]. Although Rtg1p is a necessary activator of RTG genes, its binding with Rtg3p keeps Rtg3p from flushing into the nucleus when mitochondrial damage signal is absent [14].

The retrograde response in yeast regulates the synthesis of amino-acid production and restores the mitochondrial membrane potential. The RTG pathway enables yeast to overcome unfavorable environment, such as the interference of amino acid production by anti-fungi drugs. The key role of RTG pathway is to regulate the metabolism and maintain mitochondrial quality when mitochondria are damaged by interacting the nucleus genome.

2.2 A Boolean model of mitochondrial network

To simplify the systematic behavior of mitochondrial retrograde signaling, a Boolean model is established to describe the mechanism of protein translocation associated with mitochondrial damage. In this model, The population of N mitochondria is indexed into

a vector \vec{MT} (Eq. 2.1).

$$\vec{MT} := [MT_1, \dots, MT_N] \quad (2.1)$$



Though it is known that damaged mitochondria activate Rtg2p and promotes the dephosphorylation of Rtg3p by decreasing Bmh/Mksp heterodimer [17, 14], how Rtg2p senses mitochondrial dysfunction is still unclear. Therefore, we assume mitochondria activates Rtg2p simultaneously under Michaelis-Menten kinetics [32], and the activation rate of Rtg2p is influenced by the weighted linear summation of mitochondrial damage signal (S) with their volume(Eq. 2.2).

$$S = \sum_{i=1}^N Volume_{MT_i} \cdot Damaged_{MT_i} \quad (2.2)$$

In our Boolean model, the signal (S) is set to 0 for the healthy mitochondrial population and set to 1 when mitochondria are damaged. Mitochondria in ρ^0 yeast cells have no mitochondrial DNA. These genetically damaged mitochondria have no respiratory functionality and keep activating retrograde signaling, which causes the translocation of Rtg1p and Rtg3p, when cells contain intact RTG components (Table B.2). The translocation of Rtg1p and Rtg3p can turn on retrograde response, including upregulating *CIT2* [17].

In [14], the relative nucleus concentration of Rtg1p, Rtg2p and Rtg3p in respect of the cytoplasmic one is measured by GFP labeling, deletion strains of RTG-related genes and the comparison of ρ^+ (intact mitochondrial genome) and ρ^0 cells (lost of mitochondrial genome). Therefore, the translocation event, existence of RTG component and mitochondrial functionality can be summarized into a Boolean table, which is the system behavior

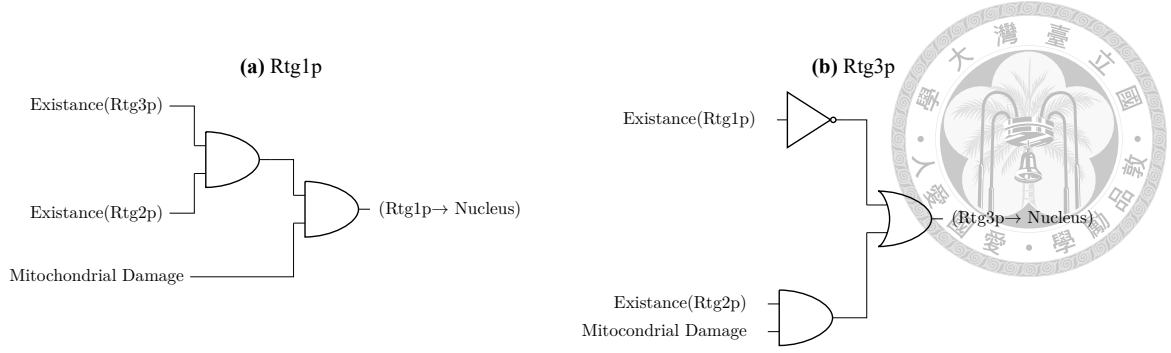


Figure 2.1. Boolean equivalent circuit of Rtg1/3p translocation.

of the RTG signaling pathway (Table B.4). The Boolean relation between mitochondrial damage (input) and the translocation of Rtg1p or Rtg3p can be further simplified with a logically equivalent.

$$\begin{aligned}
 [* - Rtg1_C] &:= [Rtg1_C] + [Rtg1 - Rtg3_C^P] + [Rtg1 - Rtg3_C^U] \\
 [* - Rtg1_N] &:= [Rtg1_N] + [Rtg1 - Rtg3_N^P] + [Rtg1 - Rtg3_N^U] \\
 [Rtg3_{\#}^*] &:= [* - Rtg3_C^*] + [* - Rtg3_N^*]
 \end{aligned} \tag{2.3}$$

2.3 The expression levels of RTG genes

The relative expression levels among RTG proteins are essential parameters for building a valid mathematical model. The initial values are derived from the Yeast GFP Database [33]. Table 2.1 represents the total concentration of each protein species. The cocentration is derived from the quantitative Western plot.

While the database lacks the expression level of Mksp. We fururther uses the microarray data from [34] (GEO access number: GSE59569) to retrieve another dataset with stress and unstress conditions (Figure B.1). These data provide the dynamical range of the

expression levels of RTG genes.



RTG Associated-proteins	Molecules per cell
Rtg1p	2190
Rtg2p	3260
Rtg3p	1050
Bmhp	158000
Mksp	<i>Not visualized</i>


Table 2.1. The expression levels of RTG proteins from the quantitative western blot. The number of molecules were measured by the quantitative Western blot from Yeast GFP Database [33]. Noted that the signal of Mksp is absent in the database possibly due to the drop of low signal intensity.

2.4 From Boolean model to ordinary differential equation-based model

In order to investigate information transmission properties, an ordinary differential equation-based model of mitochondrial retrograde signaling is developed to simulate the biological process. The differential equation-based framework of yeast RTG pathway was designed based on the knockout experiments of RTG genes (Figure 2.2).

Several assumptions were made to simplify the sophisticated protein network. The

law of conversation is applied in the form of Eq. 2.4.



$$\begin{bmatrix} Rtg1_c^{Total} \\ Rtg1_n^{Total} \\ Rtg3_c^{Total} \\ Rtg3_n^{Total} \\ Rtg2^{Total} \\ Bmh^{Total} \\ Mks^{Total} \end{bmatrix} = \begin{bmatrix} 1 & 0 & 0 & 0 & 0 & 0 & 1 & 1 & 0 & 0 & 0 & 0 & 0 & 0 & 0 \\ 0 & 1 & 0 & 0 & 0 & 0 & 0 & 0 & 1 & 1 & 0 & 0 & 0 & 0 & 0 \\ 0 & 0 & 1 & 0 & 1 & 0 & 1 & 1 & 0 & 0 & 0 & 0 & 0 & 0 & 0 \\ 0 & 0 & 0 & 1 & 0 & 1 & 0 & 0 & 1 & 1 & 0 & 0 & 0 & 0 & 0 \\ 0 & 0 & 0 & 0 & 0 & 0 & 0 & 0 & 0 & 0 & 1 & 1 & 0 & 0 & 0 \\ 0 & 0 & 0 & 0 & 0 & 0 & 0 & 0 & 0 & 0 & 0 & 0 & 1 & 0 & 1 \\ 0 & 0 & 0 & 0 & 0 & 0 & 0 & 0 & 0 & 0 & 0 & 0 & 0 & 1 & 1 \end{bmatrix} \begin{bmatrix} Rtg1_c \\ Rtg1_n \\ Rtg3_c^i \\ Rtg3_n^i \\ Rtg3_c^a \\ Rtg3_n^a \\ Rtg1/3_c^a \\ Rtg1/3_c^i \\ Rtg1/3_n^a \\ Rtg1/3_n^i \\ Rtg2_c^i \\ Rtg2_c^a \\ Bmh_c \\ Mks_c \\ Bmh/Mks_c \end{bmatrix} \quad (2.4)$$

Noted that the vector on the left hand side represents the total concentration of each protein. In our minimal model, totals of modifications are 7 from 16 RTG proteins. On the other hand, reactions of mitochondrial retrograde response are derived by the law of mass action (Eq. 2.5), Michalis-Menten kinetics (Eq. 2.6) and Hill equations (Eq. 2.7).



$$\frac{dPr_{1/2}}{dt} = k \cdot Pr_1 Pr_2 \quad (2.5)$$

$$MM(Pr, V_{max}, K_M) = \frac{dPr}{dt} = V_{max} \frac{Pr}{Pr + K_M} \quad (2.6)$$

$$Hill(Pr, V_{max}, K_M, n_H) = \frac{dPr}{dt} = V_{max} \frac{Pr^{n_H}}{Pr^{n_H} + K_M^{n_H}} \quad (2.7)$$

Where Pr denotes the concentration of a protein, k the kinetic coefficient, V_{max} maximum reaction rate, K_M Michaelis constant and n_H Hill coefficient. These are building blocks of the biological systems. The Michaelis-Menten equation (Eq. 2.6) is actually a special case of Hill equation (Eq. 2.7) when Hill coefficient (n_H) is set as 1. The Hill coefficient decides the stiffness of the reaction. Besides, the inverted Hill equation is used to describe the inhibition of Bmh/Mks heterodimer on Rtg3p activation (Eq. 2.8).

$$\frac{dPr}{dt} = V_{max} \frac{K_M^{n_H}}{Pr^{n_H} + K_M^{n_H}} \quad (2.8)$$

The activation layer consists of Rtg2p, Mksp and Bmhp, which conveys the mitochondrial damage signal by activating Rtg2p and decreases Bmhp-Mksp heterodimer which is an inhibitor of RTG pathway. Later on, Rtg1p and Rtg3p form the modulation layer. The Rtg3p contains a nuclear localization sequence (NLS), and Rtg3p is polyphosphorylated when the RTG pathway is off. On the other hand, with damaged mitochondria, Rtg3p is less phosphorylated and tends to import into the nucleus. The process of translocation of transcription factors is modeled with simplified mass kinetics (Eq. 2.9)

as mentioned in [35].



where TF_* represents transcription factor, and the subscripts $*$ describes the location with n represents nucleus and c cytoplasmic. The k_* denotes the kinetic coefficient of the translocation. With the assumption of mass equation, this reaction can be further described as an ordinary differential equation system (ODE system) (Eq. 2.10).

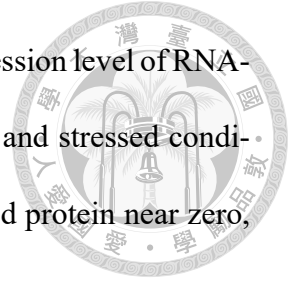
$$\begin{bmatrix} \frac{d[TC_c]}{dt} \\ \frac{d[TC_n]}{dt} \end{bmatrix} = \begin{bmatrix} 0 & k_{out} \\ k_{in} & 0 \end{bmatrix} \begin{bmatrix} [TC_c] \\ [TC_n] \end{bmatrix} \quad (2.10)$$

With the aformationed technique, the RTG pathway was described a set of ordinary differential equations that enables quantitative analysis on the mitochondrial retrograde signaling.

2.5 Parameter searching with the qualitative data of protein translocation

The parameters of Figure 2.2 determines the steady-state behavior in respect of the mitochondrial damage. A valid parameter set should make the model fulfill all conditions observed in [14] and [27] (Table B.4). The parameter set was sampled in log-uniform with fixed domain, and the relative amount of translocation kinetic coefficients is considered. To elaborate, the inward coefficient to nucleus of Rtg3p with active NLS (k_{in}^3) is higher than the inactive one (k_{in}^3). Conversely, k_{out}^3 is higher than k_{out}^3 [35].

Initial values of each component were sampled based on the expression level of RNA-seq (Figure B.1). The relative amount of protein under both normal and stressed conditions is considered. The boolean relations are tested by setting deleted protein near zero, including its modification and complexes (algorithm 1).



Once the parameters are sampled, the steady-state of the model is derived by a dynamical solver which provides an automatic switch between stiff and nonstiff algorithms when solving the differential equations. Furthermore, we chose the Order 2/3 L-Stable Rosenbrock-W method as the stiff solver, and Tsitouras 5/4 Runge-Kutta method for non-stiff section [36].

The unstable solutions are abandoned if the iteration exceeds 10^6 with a deviation of derivatives beyond 10^{-8} in total. Further, the ratio of the nucleus concentration to cytoplasmic one is used to determine the protein translocation. In our study, the nucleus-to-cytosol ratio larger than 1.5 is defined as a translocation event and vice versa. The translocation process under each deletion condition was compared with the boolean model (figure 3.1 and B.5).

The candidate parameter set were further filter out by simulating the waveform depends on the signal. The parameters which cause stiff waveform or incontinous solution with sinusoidal input signal (figure B.3) and square signal (figure B.5 and B.6) are removed. Later on, the stability are measured by screening the input domain ($input \in [0, 1]$).

To speed up the process, the Julia package *FindSteadyStates.jl* is developed to solve the steady states with multi-threading (See Section B.0.8 for details.).



Algorithm 1: Framework of finding valid parameter sets of Boolean satisfiability.

Data: Boolean relation of deletions and mitochondrial status (test conditions in table B.4)

Result: Dictionary of parameter set with Boolean satisfaction on each conditions.

while *number of trials* \leq *Maximum iteration* **do**

 Sample a parameter array with elements in the range of table 2.1;

 Shuffle the order of test conditions;

 Summing up each protein species and redistributed to one of the unbinding agent;

for $i \leftarrow 0$ to *number of conditions* **do**

if *condition*[i] *is missing* **then**

 continue;

end

foreach *deleted protein j in condition*[i] **do**

 Set protein $j \leftarrow 0$;

end

 Input \leftarrow If *Mitochondria are healthy* ? 0: 1

 Solve the steady state;

if *Solve failed* **then**

 Break;

end

 Translocations[i] \leftarrow If Nucleus GFP $\geq 1.5 \times$ Cytoplasmic GFP ? 1 : 0

if *Translocations matches with Data* **then**

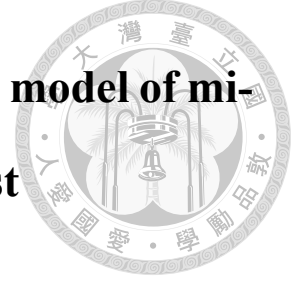
 Assign valid;

end

end

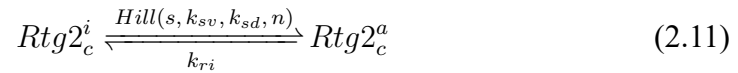
end

2.6 An ordinary differential equation-based model of mitochondrial retrograde signaling in yeast

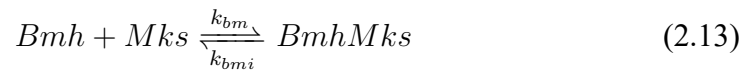
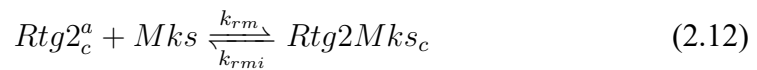


In our study, we focus on the quantitative dynamics of RTG signalling. Thus, we need a mathematical model that fullfills the current understanding and explore the system dynamics that explain further details. Our model is deterministic and majorly composed by chemical reation, Michaelis-Menten enzymatic kinetics and Hill equation. The mitochondrial damage described as input s .

1. **Modulation layer** : Rtg2p and mitochondrial damage signal (S) [15, 37]. The input layer includes the influence of mitochondrial damage on the activation of Rtg2p.

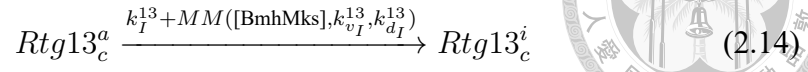


Competitive interaction between Rtg2p and Bmhp on Mksp [27].

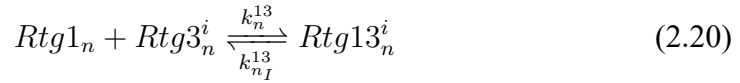
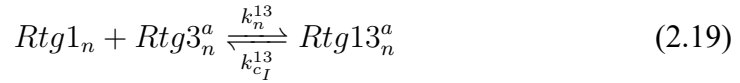
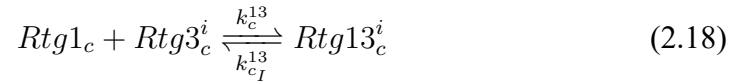
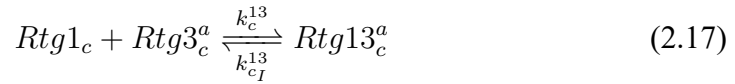


2. **Activation layer**: Translocation of Rtg3p, Rtg1p and their derivatives [14, 38].

The constant inhibition of Bmh/Mksp is described by



The formation of Rtg1/3



Translocation. Passive anchored of Rtg1p in nucleus. The heterodimer can not penetrate the nucleus membrane.



As illustrated in Figure 2.2. The input layer is composed of an inactive form of Rtg2p ($Rtg2p_C^{ina}$), and the active one ($Rtg2p_C^{act}$). Both of them are always cytoplasmic (C). As mentioned above, Rtg2p is a sensor of mitochondrial damage [39, 15, 40], and its

activation is caused by loss of mitochondrial membrane potential or insufficient ATP cytoplasmic concentration [40]. This process is modeled in the Michaelis-Menten equation [32] (See section B.0.7 for details).

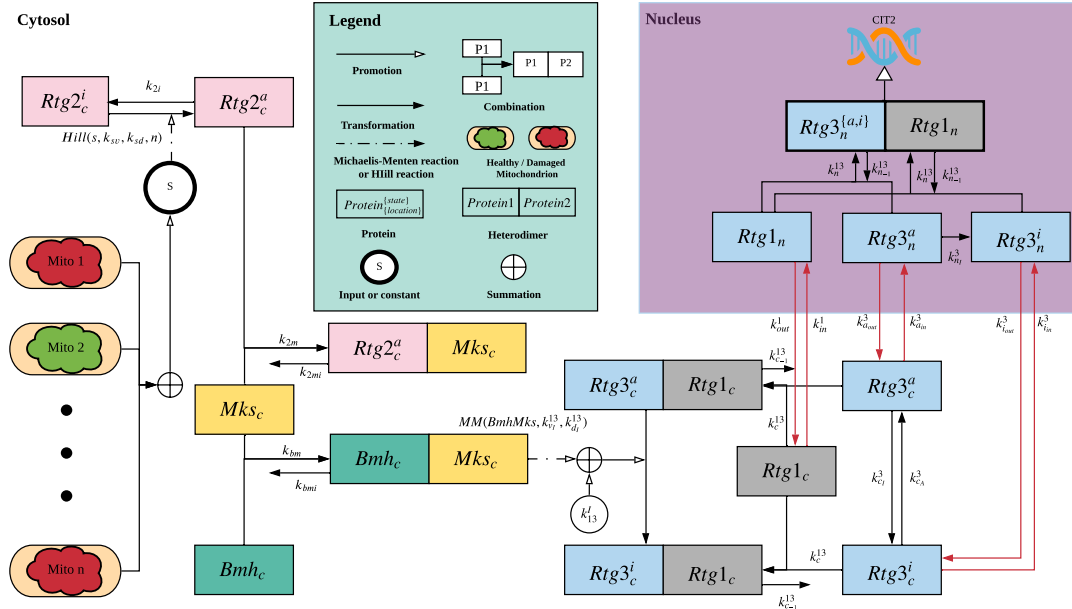
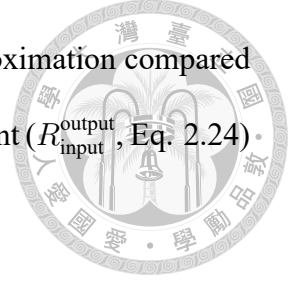


Figure 2.2. The circuit of mitochondrial-to-nucleus communication. Retrograde proteins (Bmh, Mks and Rtg1/2/3p) are divided by active (-act) and inactive state (-ina). The retrograde signaling starts with Rtg2p, which is a novel protein with an ATP binding domain similar to Hsp70/actin/sugar kinase superfamily. Rtg2p, a cytoplasmic protein, can be activated once mitochondrion loses its membrane potential or ATP concentration decreases [41, 19, 11]. The active form of Rtg2p suppresses the formation of Mks/bmh complex, an inhibitor of retrograde signaling, by binding with Mks1p, and results in the dephosphorylation of Rtg3p, which is a bHLH/Zip transcription factor associated with retrograde response genes [27, 41]. Mitochondrial retrograde response requires the presence of Rtg1p-Rtg3p complex in the nucleus. When retrograde signal is off, the Rtg3p remains phosphorylated and cytoplasmic [14]. After Bmh/Mks complex is diminished by active Rtg2p, Rtg3p tends to be dephosphorylated and translocates to nucleus accompanied by Rtg1p. The Rtg1p-Rtg3p eventually generates the retrograde response and up-regulates *CIT2* [14, 27]. The compartments are divided by nucleus (-nuc) and cytosol (-cyt). In this model, The input s is defined as the summation of mitochondrial damage signal. The arrow represents the binding of two proteins, transformation of active states or translocation between nucleus and cytosol with kinetic coefficient labelled beside.

2.7 Ultrasensitivity analysis with relative amplification approach

The relative amplification approach is applied to quantify the local and global sensitivity by estimating the equivalent Hill coefficient [42]. When the response curve starts

with a high basal level, this approach provides a more accurate approximation compared to the method using EC90:EC10 ratio [42, 43]. The response coefficient (R_{input}^{output} , Eq. 2.24) is used to quantify the relative change in response to the stimulus.



$$R_{input}^{output} = \frac{input}{output} \cdot \frac{d \text{ output}}{d \text{ input}} \quad (2.24)$$

Furthermore, to circumvent the deviation from a high basal level, the activated fraction (f , Equation 2.25) is defined as the activated ratio of output between the maximum and basal response [42].

$$f(\text{output}) = \frac{\text{output} - \text{output}_{\text{basal}}}{\text{output}_{\text{max}} - \text{output}_{\text{basal}}} \quad (2.25)$$

where $f \in [0, 1]$, output is the function of input. Besides, $\text{output}_{\text{max}}$ and $\text{output}_{\text{basal}}$ represents the maximum and minimum of outputs respectively, which makes activated fraction (f) independant from the basal activation.

The advantage of applying response coefficient (R) and activated fraction (f) is that the classical Hill equation can be converted to a linear equation (Eq. 2.26) [42].

$$R = n \cdot (1 - f) \quad (2.26)$$

$$n_R = \frac{|\int_{f_L}^{f_H} R_f^{output} df|}{|\int_{f_L}^{f_H} R_{f_{MM}}^{output} df|} \quad (2.27)$$

where f_H and f_L are maximum and minimum values of output. The local hill coefficient (n_R) can be measured by the ratio of the local sensitivity and the Michaelis-Menten

baseline (Eq. 2.6).







Chapter 3 Results

3.1 The steady states of 18 mitochondrial-related conditions are verified by the qualitative studies.

1.4×10^9 random trials were performed, and the Boolean model verifies 564 parameter sets described in Section 2.2. The best parameter set was chosen based on the criteria described in section 2.5 (See table B.6 for details). The steady states in all genetic backgrounds are listed with the Boolean model in Figure 3.1. The nucleus accumulation of GFP protein is defined as the ratio of nucleus concentration to the cytoplasmic greater than 1.5. Therefore, though the wild type with healthy mitochondria has slightly greater nucleus Rtg3-GFP, but is not considered nucleus accumulation with the ratio of 215.8/193 (nucleus/cytosol) (Figure 3.1).

With the fitted model, the Rtg3-GFP is accumulated in nucleus in $\Delta rtg1$, and this translocation is independent of the mitochondrial status. This phenomenon is consistent with the published data [14], which reveals that Rtg1p is an anchor for remaining Rtg3 cytoplasmic, but Rtg1p requires Rtg3p to translocate to the nucleus.

Notably, since $\Delta rtg2$ disconnects the mitochondrial signal with the retrograde signaling, the Δmks , which forms Bmh/Mksp and inhibits the Rtg1p/Rtg3p nucleus transloca-

tion, can override this effect as mentioned in [44]. This data is also consistent with the fitted model (Figure 3.1)

In summary, the fitted model is consistent with the known behavior of the RTG pathway and reveals the quantitative relations of the protein translocation. Because the steady states is derived with signal equals to 0 and 1. The following analysis uses the same input domain to keep the model valid with the published results in [14] and [44].

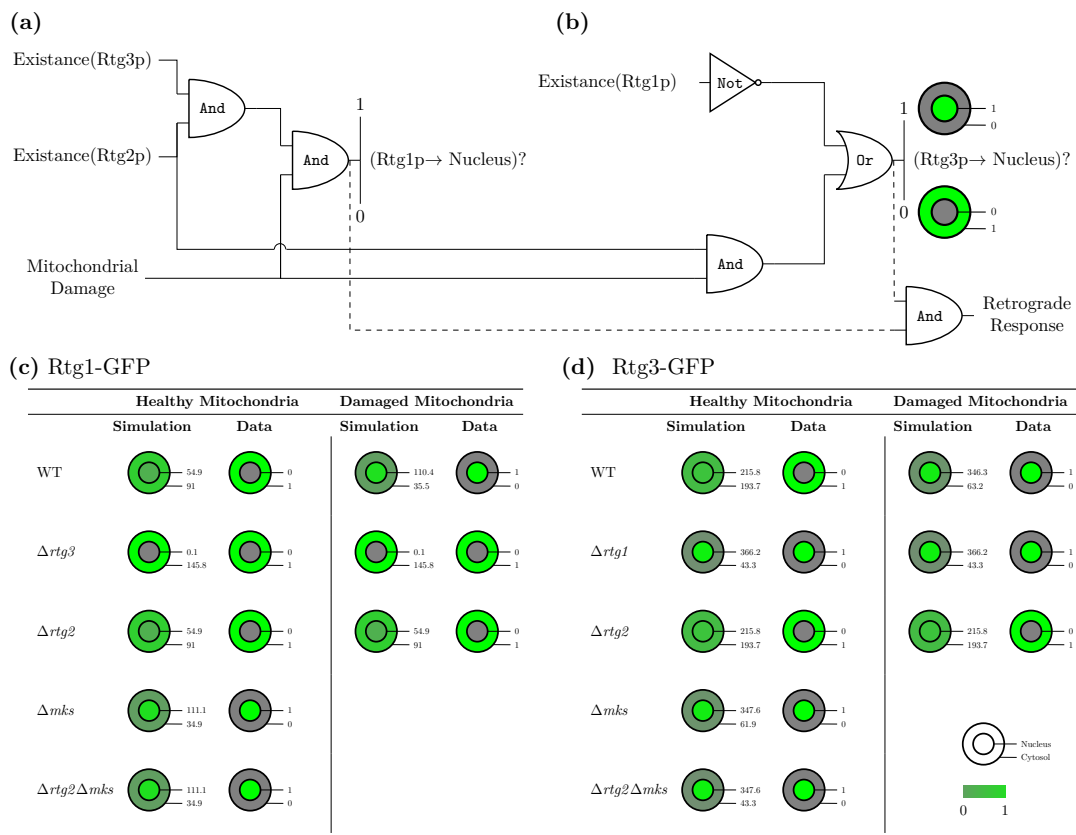
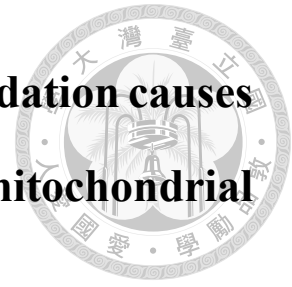


Figure 3.1. Boolean decision in RTG signaling pathway. (a) Logic gate analog for the RTG signaling pathway Rtg1p(left) and Rtg3p(right). Mitochondrial damage and the existence of Rtg1p, Rtg2p, and Rtg3p determined the translocation of Rtg1p into nucleus through a series of logic gate decisions (Table B.5). The input is defined as 0 with knockout protein or absence of mitochondrial damage, and 1 represents the existence of a protein or mitochondrial damage. On the other hand, the output is defined as 1 with nucleus accumulation and 0 means no accumulation event. The solid line represents logic gate decision for nucleus accumulation, and the dotted line represents biological process that leads to retrograde response. (b) Boolean transformation of Rtg proteins nucleus translocation in healthy and damaged mitochondria. Simulated distribution of GFP-labeled Rtg1p under multiple conditions was compared to the Boolean model. The steady states of GFP proteins are listed by the cell icon labeled with nucleus (inner circle) and cytoplasmic (outer circle) concentration in arbitrary units. Localized concentrations are described as the summation of GFP-labeled proteins, including heterodimers. The relative quantity indicates the localized concentration-to-summation ratio, from 0 (gray) to 1 (green). To verify the result, simulated distributions are compared with the qualitative data of $\Delta rtg1/\Delta rtg2/\Delta rtg3$ [14] and Δmks [41]. Nuclear accumulation is regarded as nuclear-to-cytoplasmic ratio is greater than 1.5. Simulation distribution of GFP-labeled Rtg1p (left) and GFP-labeled Rtg3p (right).

3.2 The ultrasensitivity of Bmh/Mksp degradation causes the switch-like response of Rtg1/3p to mitochondrial damage



The nucleus accumulation of Rtg1p and Rtg3p activates the retrograde response. The translocation results from mitochondrial damage, which activates Rtg2p and further induces the degradation of Bmh/Mksp. It is unclear how the information propagates from the upstream Bmh/Mksp inhibitor to the translocation of Rtg1/3p. To understand the dynamics, we apply a sigmoid signal of mitochondrial damage to simulate the transition of RTG proteins.

The step response reveals the sophisticated details about the dynamics of RTG proteins induced by a fast sigmoid transition of the damage signal (Figure 3.2). The degradation of Bmh/Mksp reveals the ultrasensitive response to the input signal. However, the translocation of Rtg1p and Rtg3p is relatively smoother and delayed. Figure 3.2 shows that the delay response of Rtg1/3p translocation occurs with a sigmoid input. On the other hand, Bmh/Mksp decreases rapidly after stimulation. The delayed stimulation of Rtg1p and Rtg3p may be caused by the slow rate of Rtg3p auto-activation for immediate response. Besides, the step response's overshoot pattern is identified in waveforms of Rtg1p and Rtg3p, while the summation cancels this effect (Figure B.3).

Two forces control the nucleus translocation of Rtg3p: the auto-activation of nuclear localization signal (NLS) and the degradation of cytoplasmic Rtg1/3p heterodimer releases extra Rtg3p monomers permeable to the nucleus membrane. When the mitochondrial damage signal degrades Bmh/Mksp via Rtg2p, the auto-activation of Rtg3p turns on

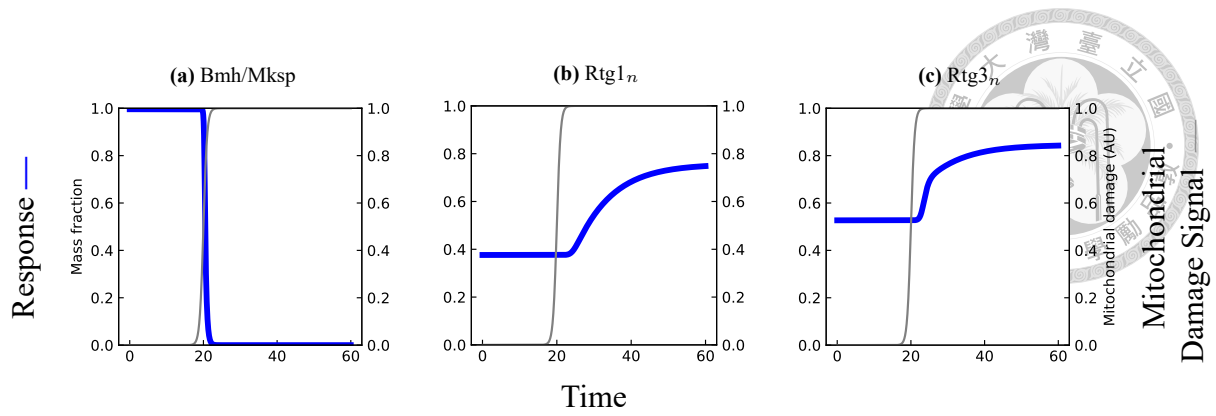
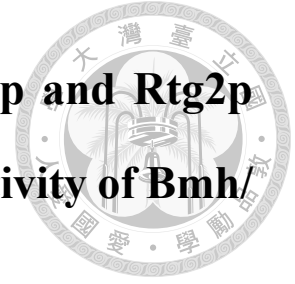


Figure 3.2. Step responses of Bmh/Mksp, Rtg1p_n and Rtg3p_n. (a) switch-like response of Bmh/Mksp (b) Capacity-charging curve with a time delay of Rtg1p_n (c) Delayed two-stage rising with sharp transition at the beginning of Rtg3p_n. The mitochondrial damage signal (thin gray line), labeled as the input with quantity shown on the right, is generated by sigmoid function with transition starting at the time (t) equal to 20 seconds, Hill coefficient equals to 2, and the domain is confined to (0,1). In response to the signal, the concentration of RTG proteins (thick blue line), regarded as outputs with quantities labeled on the left, is at a steady-state at $t = 0$. To normalize the response, the mass fraction is defined as the ratio of the concentration of a given protein set to its total concentration. Besides, the total concentration of Mks ($[Mks]_{tot}$) is used to normalize $[BmhMks]_t$.

the NLS and increases the influx kinetic coefficient. Furthermore, the overshoot of Rtg3p_c^a in concentration causes the purge in the early response (Figure B.3). The decreased cytoplasmic Rtg3p concentration further causes the degradation of Rtg1/3p heterodimer and releases more free Rtg3p. The auto-activation of Rtg3p NLS contributes to the sharp increase of Rtg3p nucleus concentration after the damage signal starts shortly. Once auto-activation reaches a steady-state, the free Rtg3p becomes conserved and translocates to the nucleus by simple diffusion. Hence, the transition of Rtg3p gets smoother in the second stage, leading to a capacity-charging curve at the end (See Figure 3.2 (c)). In addition to Rtg3p, the translocation of Rtg1p results from the degradation of cytoplasmic Rtg1/3p heterodimer and simple diffusion. Note that when Rtg1p is absent or negligible, the simple diffusion causes Rtg3p concentrated in the nucleus independent of the damage signal. The role of Rtg1p is to retain Rtg3p cytoplasmic, but the anchoring force is insufficient to retain activated Rtg3p [14]. The simulation supports the observations and provides details about the ultrasensitivity of Bmh/Mksp degradation, the two-stage transition of Rtg3p, and the capacity-charging curve of Rtg1p in response to mitochondrial damage signal.

3.3 The competitive binding between Bmhp and Rtg2p with Mksp contributes to the ultrasensitivity of Bmh/Mksp degradation



The ultrasensitivity of Bmh/Mksp degradation is identified by the phase plot with mitochondrial damage as input (Figure 3.3a). The damage signal causes the activation of Rtg2p. Although the Hill function describes this process with a dissociation constant k_{nd} , the phase plot of Rtg2p reveals a two-stage sigmoid transition with two dissociation constants significantly below k_{nd} , and with higher stiffness on the first one (Figure 3.3b). On the other hand, the degradation of Bmh/Mksp occurs at the first transition; the threshold of sensing mitochondrial damage is smaller than that of the input Hill function. Therefore, the ultrasensitivity of Bmh/Mksp is independent of the Hill input model and caused by the competitive binding between activated Rtg2p and Bmhp.

To quantify the sigmoid-like transition's sensitivity, the relative amplification method, a quantitative method for estimating the Hill coefficient with basal activation, is applied for identifying the ultrasensitivity. As shown in Figure 3.3c, the response of inactivated Rtg2p (Rtg2p^{ina}) is with decreased Hill coefficients on both of the transitions compared to the input locally and globally (Figure 3.3c, left). On the other hand, the degradation of Bmh/Mksp heterodimer occurs at the first transition of Rtg2p^{ina} , with a higher Hill coefficient and smaller than the one of input (Figure 3.3c, right). By the relative amplification method, we have estimated the Hill coefficient numerically. Despite knowing the quantity of the Hill coefficient, the transition of Bmh/Mksp occurs far below the dissociation constant k_{nd} , which is unlikely to be caused by the input Hill function, leading to the question

about the source of its ultrasensitivity.

To uncover the hidden mechanism, we have applied analytical analysis for the Rtg2p-Mksp-Bmhp motif by solving the steady states algebraically. The exact analytical solution reveals that the transitions of inactivated Rtg2p come from the molecular titration (see section 3.4 for details). Furthermore, the competitive binding between Rtg2p and Bmhp with Mksp forms a binary switch that can process the analog input signal into digital information.



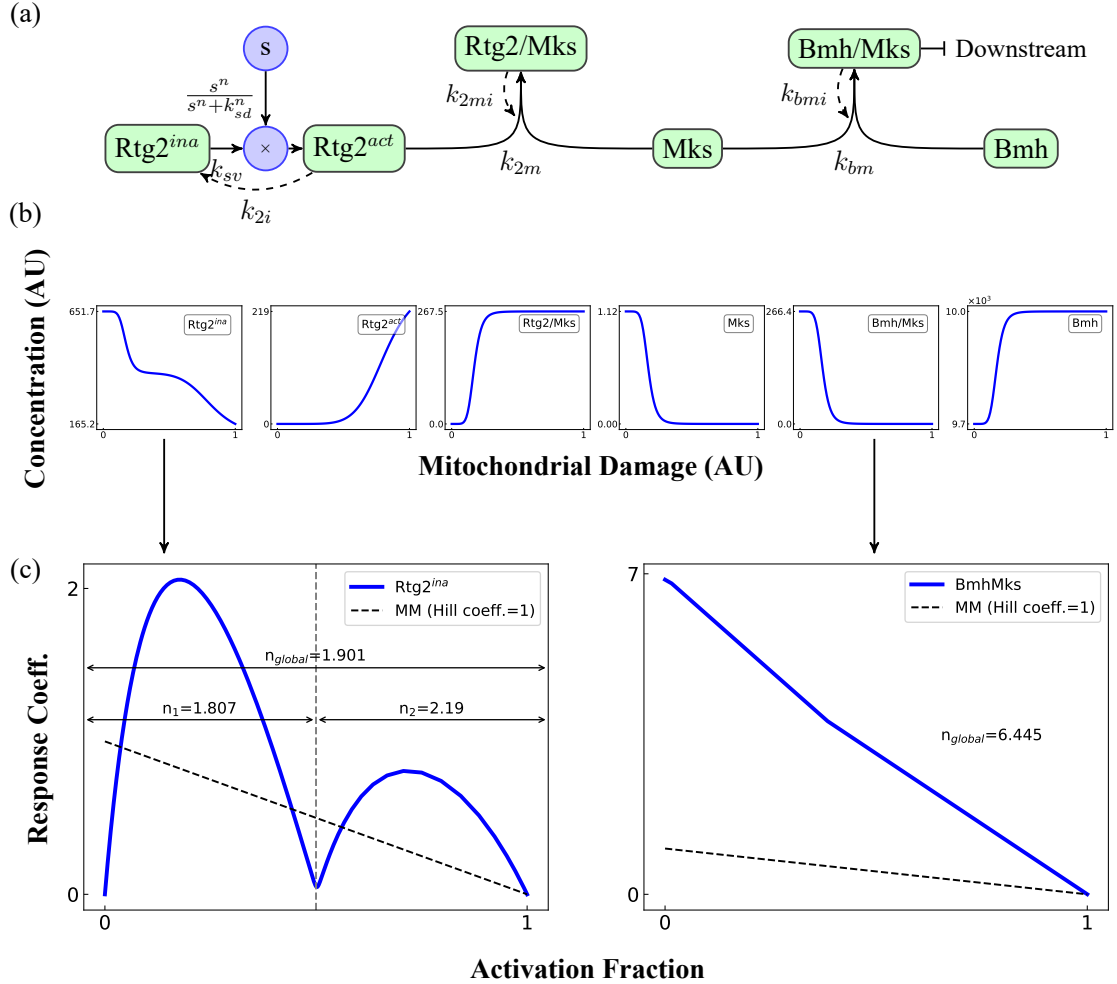


Figure 3.3. Ultrasensitivity of Bmh/Mksp heterodimer results from molecular titration. (a) Scheme of the competitive binding between Rtg2p and Bmh with Mksp. The binding reactions and transformed processes are labeled in thick arrows with one or two ends, while reverse reactions are labeled in dashed arrows. (b) Phase plots of the input responses for $n = 7$, $k_{sd} = 0.96$, $k_{sv} = 11.67$, $k_{2i} = 4.94$, $k_{2mi} = 0.043$, $k_{2m} = 1604.15$, $k_{bmi} = 2.413$, $k_{bm} = 0.059$ with arbitrary unit (AU). The input signal is defined on the interval between 0 and 1, and the corresponding steady states are plotted separately. (c) Relative amplification approach of Rtg2p^{ina} and Bmh/Mksp in response to mitochondrial damage input. The activated fraction is converted from the input signal s normalized by its range as defined in [42]; response coefficient is the normalized sensitivity of output in respect of input signal [43]. The transformed responses of Rtg2p^{ina} and Bmh/Mksp (blue thick line) are compared with the Michaelis-Menten reaction with Hill coefficient equals to one, which is a linear function (dashed line) [42]. n_{global} represents global Hill coefficient; n_1 and n_2 are local Hill coefficients in the first and second transition of Rtg2p^{ina} (See section 3.4 for details.).

3.4 Quantitative analysis of the activation layer



3.4.1 The analytical solution of the activation layer

The activation layer contains three cytoplasmic proteins: Rtg2p, Bmh1/2p and Mks1p [41, 17, 13]. A decline in mitochondrial membrane potential ($\Delta\Psi_m$) leads to the activation of Rtg2p, and further preventing the formation of Mks1p-Bmh1/2p complex which impedes the nucleus accumulation of Rtg3p by inhibiting its partial dephosphorylation [17].

The reaction is summarized in the form of competitive binding with three components. Rtg2p and Bmhp (including Bmh1p and Bmh2p) are two ligands that compete for the Mks1p (Equation 3.3). The input of the activation layer is the mitochondrial damage (s in Equation 3.3) which can be the drop of its $\Delta\Psi_m$, and further defined within continuous value between 0 and 1 which represent healthy and damaged states respectively. Further, the activation of Rtg2p induced by mitochondrial damage is modelled by a Hill equation. In the proposed model, the kinetic coefficients and total concentration of each protein are regarded as constants (Equation 3.6 and 3.9).

With the verified parameter set, we identified the two-stage transition of Rtg2p activation induced by the mitochondrial damage signal. The first stage of transition is a sigmoidal curve with the following steady region as the damage signal goes high, revealing the behavior of ultrasensitivity. After a certain value, the active form of Rtg2p increases in a convex trend and slower slope compared with the first stage of transition. Furthermore, by screening possible Hill coefficient of Rtg2p activation (n^s), we found that the threshold of the first transition, rather than the stiffness of the curve, moving higher when

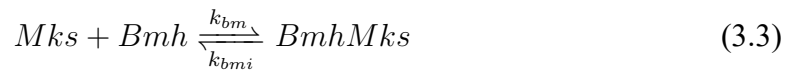
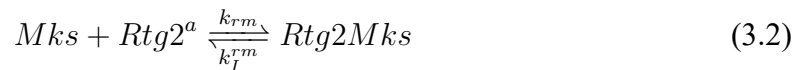
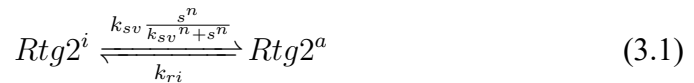
n increases.

To further understand these phenomenon, it is necessary to derive the analytical solution of steady states to understand the input-output relation of mitochondrial damage and the total concentration of Bmh/Mksp heterodimer. In the following paragraph, we used $[Rtg2_c^{act}]$, $[Rtg2_c^{ina}]$, $[Bmh]$ and $[Mks]$ to represent their steady-state concentration.



3.4.2 The competitive binding of Bmhp and Rtg2p with Mksp is the source of the ultrasensitivity.

The mechanism of ultrasensitivity is further investigated by steady state analysis. We used the modified competitive binding model from [45] with RTG protein species.



The dissociation coefficient can be further defined by the ratio of forward and reverse kinetic coefficients, which determined the steady state cocentration:

$$K_R = \frac{[Rtg2^a][Mks]}{[Rtg2Mks]} = \frac{k_{rmi}}{k_{rm}} \quad (3.4)$$

$$K_B = \frac{[Bmh][Mks]}{[BmhMks]} = \frac{k_{bmi}}{k_{bm}} \quad (3.5)$$

$$K_T = \frac{[Rtg2^i]}{[Rtg2^a]} = \frac{k_{ri}}{k_{sv} \frac{s^n}{k_{sv}^n + s^n}} \quad (3.6)$$



where K_R and K_B are the dissociation coefficient for the Mks's binding of $Rtg2p^a$ and Bmhp. For the $Rtg2p$ activation, We assume the input influences the activation of $Rtg2p^i$ in the manner of Hill formula (Eq.3.1 and Eq.3.6). To avoid zero division, we set the domain of input as $s \in (0, 1]$

The conservation rule requires that

$$[Rtg2]_0 = [Rtg2^i] + [Rtg2^a Mks] + [Rtg2^i] \quad (3.7)$$

$$[Bmh]_0 = [Bmh] + [BmhMks] \quad (3.8)$$

$$[Mks]_0 = [Mks] + [Rtg2^a Mks] + [BmhMks] \quad (3.9)$$

where $[Rtg2_c^a]_0$, $[Bmh]_0$ and $[P_0]$ represent total concentration, and assume they are constant. Therefore, we can make $[Bmh]$ and $[Rtg2^a Mks]$ into the dependent variables of $[Mks]$ and their total concentration.

$$[BmhMks] = \frac{[Mks][Bmh]_0}{K_B + [Mks]} \quad (3.10)$$

$$[Rtg2^a Mks] = \frac{[Rtg2_c^a]_0 [Mks]}{\frac{K_R(1+K_T)}{K_T} + [Mks]} \quad (3.11)$$

To derive the polynomial function of $[Mks]$, Let's put Eq.3.10, Eq.3.11 and Eq.3.9 together:



$$\begin{aligned}
[Mks]_0 &= [Mks] + [Rtg2^a Mks] + [Bmh Mks] \\
&= [Mks] + \frac{[Mks][Rtg2_c^a]_0}{K_R(1 + \frac{1}{K_T}) + [Mks]} + \frac{[Mks][Bmh]_0}{K_B + [Mks]} \\
&= [Mks] + \underbrace{\frac{[Mks][Rtg2_c^a]_0}{K'_R + [Mks]}}_{=[Rtg2^a Mks]} + \underbrace{\frac{[Mks][Bmh]_0}{K_B + [Mks]}}_{=[Bmh Mks]} \tag{3.12}
\end{aligned}$$

where $K'_R = K_R(1 + \frac{1}{K_S})$ is the dissociation coefficient influenced by the input coefficient K_T (Eq.3.6). Finally we can get the cubic polynomial equation of $[Mks]$ from Eq.3.12:

$$[Mks]^3 + a[Mks]^2 + b[Mks] + c = 0 \tag{3.13}$$

where

$$\begin{aligned}
a &= K'_R + K_B + [Rtg2_c^a]_0 + [Bmh]_0 - [Mks]_0 \\
b &= K_B([Rtg2_c^a]_0 - [Mks]_0) + K'_R([Bmh]_0 - [Mks]_0) + K'_R K_B \\
c &= -K'_R K_B [Mks]_0
\end{aligned}$$

The polynomial equation of $[Mks]$ can be solved by applying trigonometry [45],

The analytical solution of competitive ligand binding

$$[Mks] = -\frac{a}{3} + \frac{2}{3}\sqrt{(a^2 - 3b)}\cos\frac{\theta}{3} \tag{3.14}$$

$$[Rtg2Mks] = \frac{[Rtg2]_0(2\sqrt{a^2 - 3b} \cos(\theta/3) - a)}{3K_R + 2\sqrt{(a^2 - 3b)} \cos(\theta/3) - a} \quad (3.15)$$

$$[BmhMks] = \frac{[Bmh]_0(2\sqrt{a^2 - 3b} \cos(\theta/3) - a)}{3K_B + 2\sqrt{(a^2 - 3b)} \cos(\theta/3) - a} \quad (3.16)$$

$$[Bmh] = [Bmh]_0 - [BmhMks] \quad (3.17)$$

$$[Rtg2^a] = ([Rtg2]_0 - [Rtg2Mks]) \frac{1}{1 + K_T} \quad (3.18)$$

$$[Rtg2^i] = ([Rtg2]_0 - [Rtg2Mks]) \frac{K_T}{1 + K_T} \quad (3.19)$$

$$\text{where } \theta = \cos^{-1}\left(\frac{-2a^3 + 9ab - 27c}{2\sqrt{(a^2 - 3b)^3}}\right).$$

The analytical solution demonstrates the the sigmoid curve is restulted from the in-verse cosine function, a sigmoid-like function, caused by the competitive binding between Bmhp and Rtg2p with Mksp.

3.5 Frequency modulation of mitochondrial retrograde signaling

In addition to the binary response, we further investigate the input-output relation-ship in the frequency domain. Figure 3.4 reveals the frequency modulation of Bmh/Mksp heterodimer, nucleus Rtg1p and Rtg3p in response to sinusoidal damage signal with mul-tiple frequencies. All of them reveal the behavior as a low pass filter. The recovery rate of Bmh/Mksp synthesis is significantly slower than the degradation (Figure 3.4 (a)), leading to a sign sensitive delay which keeps the switch on after the damage is once detected [46], while Bmh/Mksp can still slowly synthesize for a long period of around 3×10^3 seconds compared to the transition in less than 10 seconds (See Figure B.5 (a)).



On the other hand, though the concentration of Bmh/Mksp slowly recovers after stimulation, Rtg1p and Rtg3p are still able to convey the dynamics of an input signal (Figure 3.4 (b) and 3.4 (c)). In low frequency, both reach high and low saturation states in a sinusoidal input cycle and produce a square wave pattern. As the frequency goes high, the amplitude of output diminishes with drifting, revealing mitochondrial damage signal is low-pass filtered by the retrograde signaling. Moreover, the delay of Rtg's translocation may contribute to the instability, and destroy the robustness.

To investigate the feedback instability of mitochondrial retrograde signaling, we further derive the Bode plot of retrograde response in the stationary stage (Figure 3.5). In the frequency response of Bmh/Mksp, the gain decreases in two sections separated by $10^{-0.5}$ Hz. The gain of the section of high frequency decreases more rapidly than the one of low frequency, and the phase delay also increases significantly in the high-frequency region. On the other hand, the cutoff frequency of nucleus Rtg1p and Rtg3p locates at around 10^{-2} Hz as low-pass filters. For nucleus Rtg3p, there is a second cutoff frequency at around $10^{-0.5}$ Hz with a more rigid negative slope. In addition to the gain modulation, both of nucleus Rtg1p and Rtg3p reveals four sections of phase delay with increasing rigidity of slope as input frequency increases, and both shares similar cutoff frequencies at $10^{-2.5}$, 10^{-2} and 10^{-1} approximately in phase delay (See the phase plots in Figure 3.5 (b) and 3.5 (c)).

Finally, we apply the Nyquist stability theorem for identifying the closed-loop stability of mitochondrial retrograde signaling (See Nyquist section of Figure 3.5). Despite phase delay, the mitochondrial retrograde signaling remains stable in response to the damage signal [47]. The phase and gain margin derived from the Bode plots can further indicate the tolerance of delay when retrograde signaling connects to the cellular response.

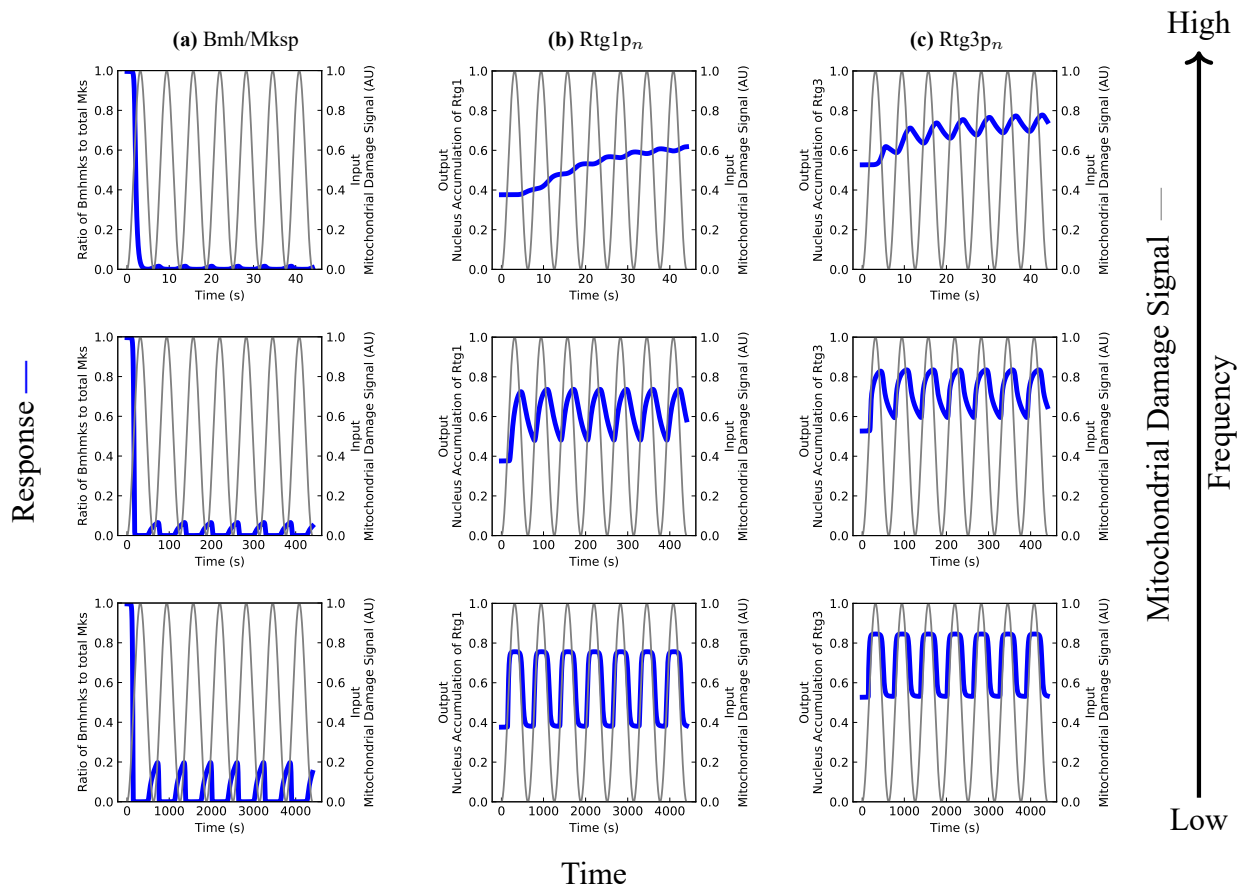


Figure 3.4. The frequency response of mitochondrial damage signal and RTG protein concentrations. The sinusoidal inputs (gray thin curves) with 1.6×10^{-3} Hz (bottom), 1.6×10^{-2} Hz (middle) and 1.6×10^{-1} Hz (top) reveals RTG signalling pathway as a low-pass filter. (a) Response of Bmh/Mksp (blue thickened curve) (b, c) Response of Rtg1pn and Rtg3pn (blue thickened curves). The y-axis represents the nucleus accumulation induced by the input signal, and the quantity is described by the ratio of nucleus concentration to total protein concentration.

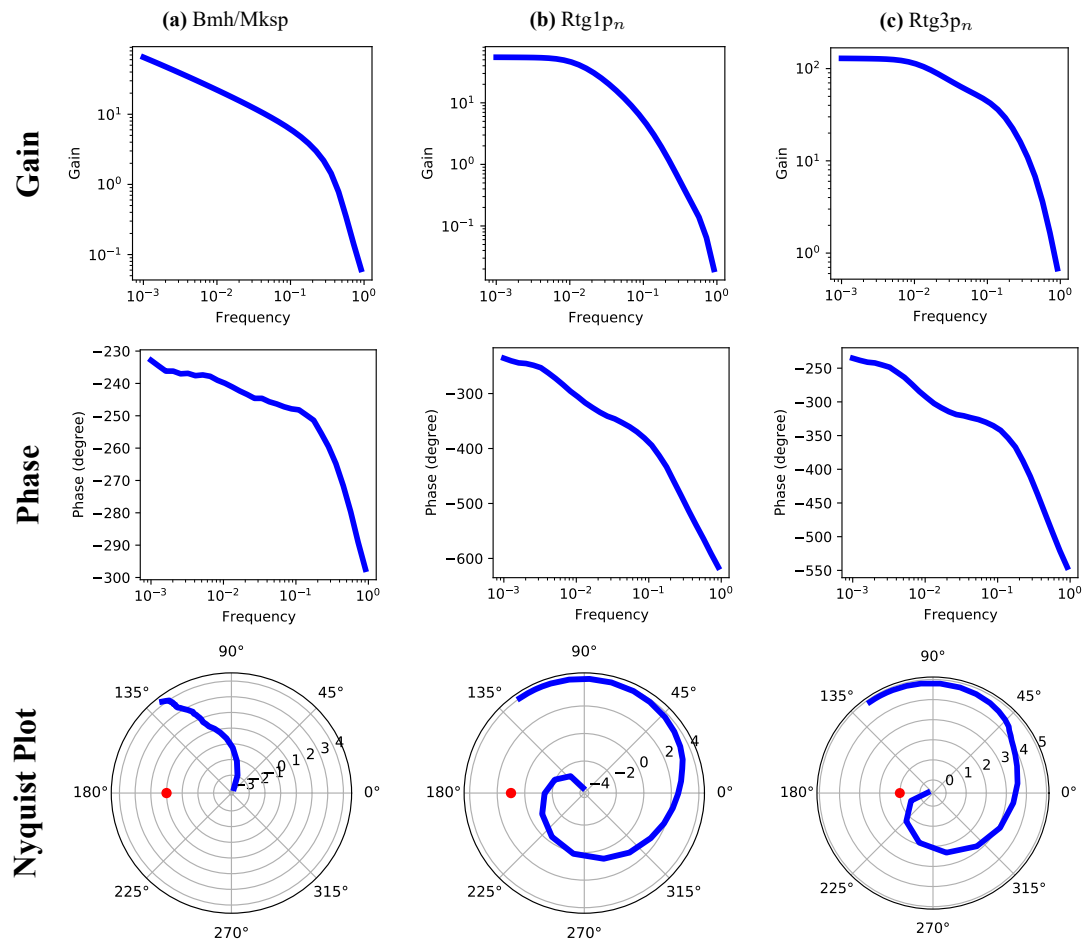


Figure 3.5. The frequency analysis of Bmh/Mksp, Rtg1pn and Rtg3pn in respect of mitochondrial damage. In the Nyquist plots (row 3), the red dot represents the critical point $(-1 + 0j)$, and the responses are labelled in blue dots. Noted that the radius represents the gain with log scale. The gain is measured when the oscillation reaches a stationary phase.

3.6 Robustness analysis



To understand how noise influences the robustness along with the damage signal, the ODE model is further extended to the Chemical Langevin equations (Eq. 3.20). The stochastic model incorporates the random process into a deterministic model, and the potential landscape of the nucleus Rtg1/Rtg3p is derived by screening the damage input with ensemble simulations (Figure 3.6).

$$d[Rtg13_n]_t = \underbrace{\sum_{r=1}^R S_r f_r([Rtg13_n]_t) dt}_{\text{Drifting}} + \underbrace{\sqrt{\sum_{r=1}^R S_r^2 f_r([Rtg13_n]_t)} dW}_{\text{Diffusion}} \quad (3.20)$$

where f_r is the propensity of r^{th} reaction, S_r the net change of the reaction r , and dW represents the Wiener process [48].

Along with the damage signal, the sigmoid curve of the potential landscape is consistent with the deterministic results of Rtg1/Rtg3p (Figure 3.6 (a)/B.4 (a)). Interestingly, the conjugated steady states are identified with the yellow bands and the sigmoid curve (Figure 3.6 (a)). This structure becomes distanced as the input signal increases, indicating the noise is amplified and causes larger bandwidth as the signal increases, leading to a compromised signal-to-noise ratio.

Notably, three conjugated steady states are further investigated by measuring the output distribution in a given input (Figure 3.6 (b)). Three conjugated steady states are identified by the peak of the probability, which represents the high likelihood of the Rtg1/Rtg3p concentration in a given input. The conjugated steady states are located within the band-

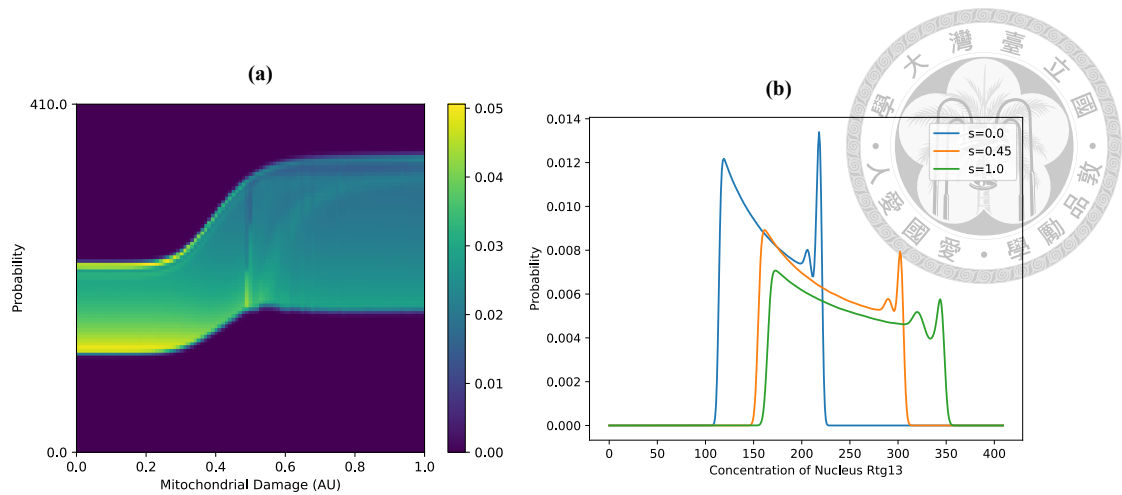


Figure 3.6. (a) The potential landscape of nucleus Rtg1/Rtg3p responds to mitochondrial damage signal. The sigmoid transition is identified in Figure B.4 (a), but the bandwidth (the yellowish area in the vertical section) is increased along with the damage signal. The damage signal is sampled in 100 grids and assigned to the chemical Langevin model to simulate the stochastic process. Every combination of parameters is applied with 100-time length (arbitrary unit) with automatic time step. The y-axis is limited on the range of 0 and the maximum concentration of Rtg3p. A heatmap shows the probability with a color bar on the right side. (b) The probability density function (PDF) in respect of Rtg1/Rtg3p influenced by damage signal. The distribution is simulated by setting the input signal as 0 (blue, minimal input), 0.45 (orange, intermediate input), and 1 (green, maximum input). The peaks represent three stable steady states, and the valley between the right two high peaks is the saddle point. The PDF is measured by time-series simulation and estimates the probability with kernel density estimation.

width of the probability density function (PDF), and the length of bandwidth is increased by the signal as shown in Figure 3.6 (b). This result suggests that the mitochondrial retrograde signal is not only a bistable model but a toggle-switch with three locally conjugated stable steady states and one saddle point (Figure 3.6 (b)). Also, the uncertainty of the output is compromised by a high input signal, which may deteriorate the mutual information between mitochondria and the nucleus when mitochondria keep sending the message of high intensity.

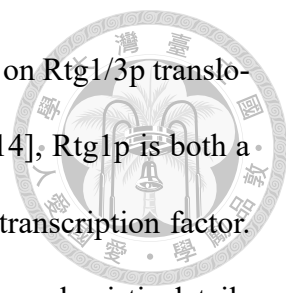




Chapter 4 Discussion

We have constructed a novel mathematical model of mitochondrial retrograde signaling in yeast and apply to microscopic data of RTG knockout experiments with expression data for validation. The differential equation-based model provides a profound mechanism to the dynamical response of mitochondrial retrograde signaling, which is difficult to derive from experiments due to the lack of precise manipulation of mitochondrial quality in real-time. The dynamics of the retrograde signaling are revealed by injecting the input signal with step and sinusoidal waveforms. Moreover, we apply an analytical solution to identify the source of ultrasensitivity in the degradation of Bmh/Mksp heterodimer.

The switch-like behavior of yeast mitochondrial retrograde signaling is described in [11]. In our retrograde model (Figure 2.2), we support the idea with both exact mathematical formula and numerical simulation. We identify the switch-like behavior results from the competitive binding between active Rtg2p and Bmh. Besides, the effect of molecular titration causes the two-stage transition in inactive Rtg2p. The ultrasensitivity is typical in cellular communication, allowing cells to remove noise and amplify the input signals [49, 50, 51]. The Rtg2p senses the mitochondrial quality with the modulation of Bmhp and Mksp, forming a digital detector via competitive binding. The "all-or-none" response can further filter fluctuation and adjust to the unpredictable environment.



This study further elaborates the properties of signal modulation on Rtg1/3p translocation with static and sinusoidal damage signals. As mentioned in [14], Rtg1p is both a positive and negative regulator, which keep Rtg3p cytoplasmic as a transcription factor. This majorly constraint the valid parameter set (See Table B.6). More mechanistic details are found by the proposed model: The two-stage transition of Rtg3p translocation in step response and the sign-sensitive delay of Rtg3p with short ON delay in oscillation signal. On the other hand, without the modification of the nuclear localization signal. The existence of Rtg1p is necessary to keep Rtg3p cytoplasmic when mitochondrial damage signal is absent, which is one of the criteria of our model (See Table B.1). Rtg1p provides an anchoring effect on Rtg3p via forming heterodimer, which may be impermeable to the nucleus membrane. The translocation of Rtg1p is insensitive to the sign of the input change and reveals a simple diffusion process with a capacity-charging pattern. The frequency response further shows the low-pass filtering of the RTG pathway, which can reject high-frequency fluctuations and retain the overall information of the input signal for requesting nucleus supply (Figure 4.1).

Further, the robustness analysis reveals that the intensity of input signal can diminish the robustness, making the communication system unstable. Recent studies have shown that mitochondrial membrane potential oscillation occurs under semi-anaerobic conditions or continuous culture in budding yeast [52, 53, 54]. Moreover, mitochondria undergo energization cycles driven by ultradian clock, contributing to respiratory oscillations in yeast [55, 56, 57, 58]. The respiratory oscillations may be a source of reactive oxygen species generated by mitochondria [57]. In our study, we further explore the feedback stability by Bode and Nyquist diagram [47, 59], revealing the feedback stability of the retrograde signaling. The mito-nucleus communication is a two-way process [60]: The retrograde

signaling is connected to glutamate synthesis, mTOR signaling, and other feedback circuits [61, 13, 5]. The phase and gain margin in the Bode plot determines the stable region when cascading with these functional units under the mitochondrial oscillation.

Recent studies have shown that mitochondrial membrane potential oscillation occurs under semi-anaerobic conditions or continuous culture in budding yeast [52, 53, 54] and the insulin secretion of the pancreatic cell [62]. Moreover, mitochondria undergo energization cycles driven by ultradian clock, contributing to respiratory oscillations of mitochondria [55, 56, 57, 58]. These oscillations may be a source of reactive oxygen species generated by mitochondria [57], and further interfere the retrograde signaling with sinusoidal input. Our model elucidates how the RTG pathway processes the input signal as a low-pass filter and reports status to the nucleus genome, which may support the synchronization of mitochondrial membrane potential in yeast [54, 55] and in the related mechanism of insulin secretion [62]

The mitochondrion is a hub of biochemical pathways in eukaryotic cells [63]. Instead of energy acquisition, this semi-autonomous organelle also participates various metabolic reactions which relates to aging [64, 65, 66], cellular communication [3, 62] and cell viability [26, 28]. The RTG pathway is the key to cell adaptation and provides cytoprotection via metabolic reprogramming [25, 4]. The robustness of retrograde signaling is essential for adjusting the unfavorable environment [26]. For instance, RTG signaling also contributes to drug resistance in pathogenic yeast such as *C. albicans* which causes around 80% of major systemic fungal infections [25, 67]. Many antifungal drugs target mitochondrial-related metabolisms of amino-acids and ergosterol [68, 69], while the retrograde pathway enables the pathogenic yeast to overcome the toxics by sensing the loss of mitochondrial functionality and reprogram the metabolism [70, 30, 25]. Hence, the

yeast retrograde signaling has become a potential target for developing antifungal drugs [25]. However, how yeast senses mitochondrial stress via the RTG pathway in a fluctuated environment remains unclear.



In this study, we have applied mathematical modeling to unravel the dynamics of retrograde signaling from a control-system point of view. We further identify the threshold of RTG response, which can be used for the optimal dosage design to eliminate the pathogenic yeast without turning on the retrograde signaling. Also, the frequency response reveals how yeast manages to the fluctuation by the low-pass filtering of RTG pathway, and the hysteresis effect which keeps retrograde signaling on when the damage signal fluctuates, indicating the persistent dosage with concentration slightly below the threshold of RTG response is the optimal strategy against the pathogenic yeast. Therefore, understanding the qualitative properties of retrograde signaling may shed light on the antifungal strategy.

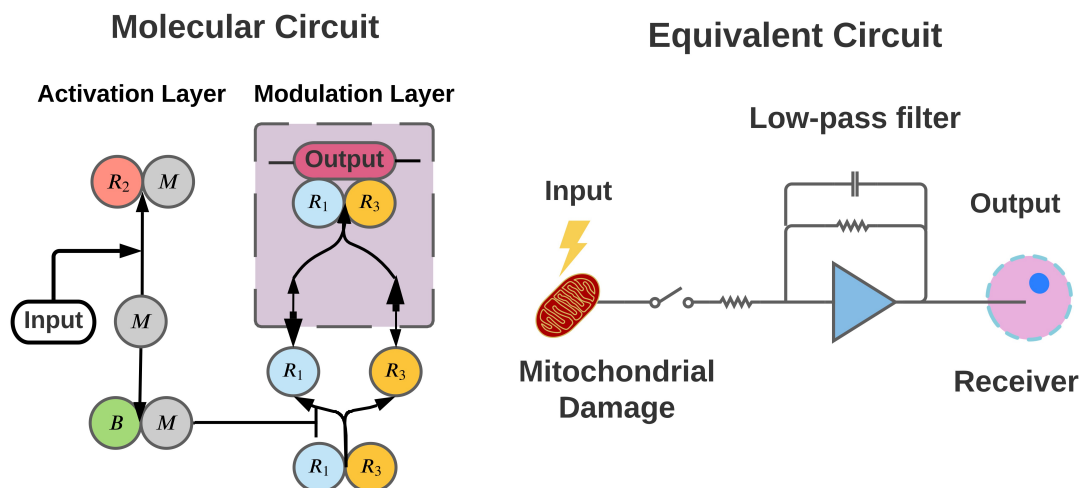


Figure 4.1. Mitochondrial retrograde circuit (a) Mitochondrial retrograde signaling facilitates communication between mitochondria and the nucleus. The retrograde molecular circuit transduces the signal through the activation layer and the modulation layer to sense and to report the signal to the nucleus. (b) Retrograde signaling circuit was switched on by a mitochondrial damage signal, while a low-pass filter maintained the robustness of the pathway.



Chapter 5 Concluding Remarks

5.0.1 Significance of this study

A mathematical model of mitochondrial retrograde signaling is proposed and examines the protein network's signal modulation in this thesis. The purpose of this study is to integrate the current understanding of mitochondrial retrograde signaling and investigate the systemic mechanisms of signal transduction. The study starts with the pioneering works of [14] and [44], which elaborates the protein-protein interactions of the retrograde signaling in yeast. A Boolean model further summarized their results, focusing on the nucleus translocation of Rtg1p and Rtg3p. The boolean model is used as the bridge between qualitative experiments and the ODE-based modeling. The ODE model parameters are found by applying a random search for solving the Boolean Satisfiability Problem and further evaluating the modulation of mitochondrial damage signal.

With the proposed ODE model, the ultrasensitivity of retrograde signaling in response to mitochondrial damage is identified, and further steady-state analysis reveals this effect results from the competitive binding of Rtg2p and Bmhp with Mksp. Later on, the dynamical input is used to elaborate the frequency modulation. The low-pass effect with delay is identified, but the signaling systems remain stable, proved by the Nyquist criterion.

Further, the robustness of the model is investigated by extending the ODE model to Chemical Langevin Equations (Eq. 3.20). The signal-to-noise ratio is compromised as the mitochondrial damage signal increases, revealing the asymmetric robustness of the bistable model with the mitochondrial damage as an input. By applying the stochastic approach, we also identified the potential landscape of the proposed ODE model. There are three steady states in one given input, and their locations drifting and distancing in response to the damage signal.

Notably, the computational work of this study is written mostly by the Julia programming language. *FindSteadyStates.jl*, a package for exploring steady states with multithreading, is published to support the growing community. Another two packages - *EstimHill.jl* for ultrasensitive analysis with relative amplification approach, and *PotentialMap.jl* for estimating the potential landscape of nonlinear ODE equations are developed and will be finish as mature packages (See B.0.8).

This study has proposed the first mathematical model of mitochondrial retrograde signaling in yeast with ODE. We further extend the findings to possible applications against the pathogenic yeast. We hope the quantitative study on mitochondrial quality control can help the development of antifungal therapy.

5.0.2 Limitation

Even though this study has been designed to model the retrograde signaling from mitochondria to the nucleus. This model doesn't include the broader aspect on the feedback response and multiple genetic regulation results from the activation of Rtg1p and Rtg3p. We mainly focus on the one-way reaction at a short period and neglect the change

of protein concentrations.

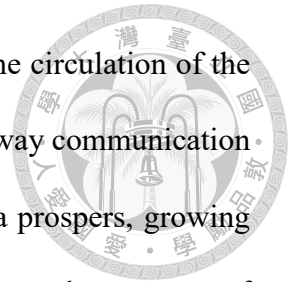
On the other hand, the definition of mitochondrial damage is not unique in this model because how Rtg2p senses mitochondrial damage is still unclear. A Hill equation is used to summarize the effect on Rtg2p activation. Notably, a recent study has shed light on the possible mechanism of mitochondrial-related Rtg2p activation, caused by the ATP binding site on Rtg2p structure. This structural finding provides a possible explanation of how Rtg2p is influenced by mitochondrial dysfunction, which usually decreases the ATP/ADP ratio.

Last but not least, although this is the minimal model of the mitochondrial retrograde signaling, it has explained why retrograde signaling has the switch-like properties in response to mitochondrial damage mentioned in [11]. The theoretical model can further explore the systemic dynamics, which is challenging to be reached by experiments. This model provides flexibility and allows to extend to a more significant scenario of the metabolic networks.

5.0.3 Future perspective

To fully understand the communication between mitochondria and the nucleus. This model needs to include multiple mitochondria as signal sources, forming a multiple-input-single-output (MISO) system. Using the Chemical Langevin Model, the information flow can be estimated in bits, and the influences of mitochondrial fission-fusion can be modeled with the retrograde signaling. The agent-based modeling can provide a coarse-grained method to simulate the mitochondrial dynamics. What nucleus received from multiple mitochondria can be further elaborated.

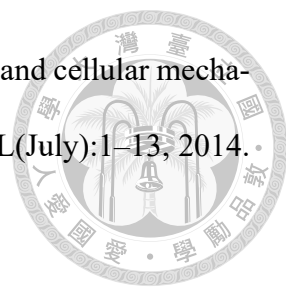
Besides, the feed-forward signaling can be added to complete the circulation of the communication. The mitochondrial quality control relies on the two-way communication between mitochondria and the nucleus. As the field of mitochondria prospers, growing data about mitochondrial imaging and expression data can further support the accuracy of the simulation. The ultimate goal of this study is to discover the target site for antifungal drugs.




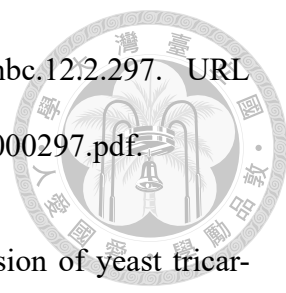


References

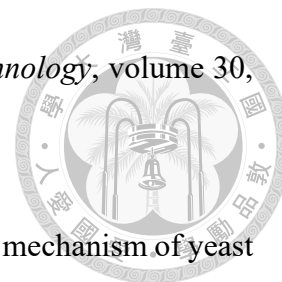
- [1] Laura D. Osellame, Thomas S. Blacker, and Michael R. Duchon. Cellular and molecular mechanisms of mitochondrial function. *Best Practice and Research: Clinical Endocrinology and Metabolism*, 26(6):711–723, 2012. ISSN 15321908. doi: 10.1016/j.beem.2012.05.003. URL <http://dx.doi.org/10.1016/j.beem.2012.05.003>.
- [2] Jonathan R. Friedman and Jodi Nunnari. Mitochondrial form and function. *Nature*, 505(7483):335–343, 2014. ISSN 0028-0836. doi: 10.1038/nature12985. URL <http://www.nature.com/nature/journal/v505/n7483/full/nature12985.html>.
- [3] Adrienne Mottis, Sébastien Herzig, and Johan Auwerx. Mitocellular communication: Shaping health and disease, 11 2019. ISSN 10959203. URL <http://science.sciencemag.org/>.
- [4] Maša Ždravlević, Nicoletta Guaragnella, Lucia Antonacci, Ersilia Marra, and Sergio Giannattasio. Yeast as a Tool to Study Signaling Pathways in Mitochondrial Stress Response and Cytoprotection. *The Scientific World Journal*, 2012:1–10, 2012. ISSN 1537-744X. doi: 10.1100/2012/912147.
- [5] Zhengchang Liu and Ronald a Butow. Mitochondrial retrograde signaling. *Annual review of genetics*, 40:159–185, 2006. ISSN 0066-4197. doi: 10.1146/annurev.genet.40.110405.090613. URL <http://www.ncbi.nlm.nih.gov/pubmed/16771627>.

- 
- [6] Miguel A. Aon, Niraj Bhatt, and Sonia Cortassa. Mitochondrial and cellular mechanisms for managing lipid excess. *Frontiers in Physiology*, 5 JUL(July):1–13, 2014. ISSN 1664042X. doi: 10.3389/fphys.2014.00282.
- [7] Nicola King. Amino acids and the mitochondria. In *Mitochondria*, pages 151–166. Springer, 2007.
- [8] Dmitry Knorre, Svyatoslav Sokolov, Anna Zyrina, and Fedor Severin. How do yeast sense mitochondrial dysfunction? *Microbial Cell*, 3(11):401–408, 2016. ISSN 23112638. doi: 10.15698/mic2016.11.537. URL <http://microbialcell.com/researcharticles/how-do-yeast-sense-mitochondrial-dysfunction/>.
- [9] Toni Gabaldón and Martijn A. Huynen. Shaping the mitochondrial proteome. *Biochimica et Biophysica Acta - Bioenergetics*, 1659(2-3):212–220, 2004. ISSN 00052728. doi: 10.1016/j.bbabbio.2004.07.011.
- [10] Carl Malina, Christer Larsson, and Jens Nielsen. Yeast mitochondria: An overview of mitochondrial biology and the potential of mitochondrial systems biology. *FEMS Yeast Research*, 18(5):1–17, 2018. ISSN 15671364. doi: 10.1093/femsyr/foy040.
- [11] Fernanda Marques Da Cunha, Nicole Quesada Torelli, and Alicia J. Kowaltowski. Mitochondrial Retrograde Signaling: Triggers, Pathways, and Outcomes. *Oxidative Medicine and Cellular Longevity*, 2015, 2015. ISSN 19420994. doi: 10.1155/2015/482582.
- [12] Umut Cagin and José Antonio Enriquez. The complex crosstalk between mitochondria and the nucleus: What goes in between? *International Journal of Biochemistry and Cell Biology*, 63(February):10–15, 2015. ISSN 18785875. doi: 10.1016/j.biocel.2015.01.026. URL <http://dx.doi.org/10.1016/j.biocel.2015.01.026>.

- 
- [13] Ronald A. Butow and Narayan G. Avadhani. Mitochondrial signaling: The retrograde response. *Molecular Cell*, 14(1):1–15, 2004. ISSN 10972765. doi: 10.1016/S1097-2765(04)00179-0.
- [14] T Sekito, J Thornton, and R A Butow. Mitochondria-to-nuclear signaling is regulated by the subcellular localization of the transcription factors rtg1p and rtg3p. *Molecular biology of the cell*, 11(6):2103–15, 6 2000. ISSN 1059-1524. doi: 10.1091/mbc.11.6.2103.
- [15] Xinsheng Liao and Ronald A. Butow. RTG1 and RTG2: Two yeast genes required for a novel path of communication from mitochondria to the nucleus. *Cell*, 72(1): 61–71, 1993. ISSN 00928674. doi: 10.1016/0092-8674(93)90050-Z.
- [16] Anna Chelstowska, Zhengchang Liu, Yankai Jia, David Amberg, and Ronald A. Butow. Signalling between mitochondria and the nucleus regulates the expression of a new D-lactate dehydrogenase activity in yeast. *Yeast*, 15(13):1377–1391, 1999. ISSN 0749503X. doi: 10.1002/(SICI)1097-0061(19990930)15:13<1377::AID-YEA473>3.0.CO;2-0.
- [17] S. Michal Jazwinski and Andres Kriete. The yeast retrograde response as a model of intracellular signaling of mitochondrial dysfunction. *Frontiers in Physiology*, 3 MAY(May):1–12, 2012. ISSN 1664042X. doi: 10.3389/fphys.2012.00139.
- [18] Charles B. Epstein, James A. Waddle, W. Hale IV, Varshal Davé, Janet Thornton, Timothy L. Macatee, Harold R. Garner, Ronald A. Butow, Walker Hale Iv, Varshal Davé, Janet Thornton, Timothy L. Macatee, Harold R. Garner, and Ronald A. Butow. Genome-wide responses to mitochondrial dysfunction. *Molecular Biology of the*

- 
- Cell*, 12(2):297–308, 2001. ISSN 10591524. doi: 10.1091/mbc.12.2.297. URL <https://www.ncbi.nlm.nih.gov/pmc/articles/PMC30944/pdf/mk000297.pdf>.
- [19] Z Liu and R a Butow. A transcriptional switch in the expression of yeast tricarboxylic acid cycle genes in response to a reduction or loss of respiratory function. *Molecular and cellular biology*, 19(10):6720–8, 1999. ISSN 0270-7306. doi: 6720–6728. URL <http://www.pubmedcentral.nih.gov/articlerender.fcgi?artid=84662&tool=pmcentrez&rendertype=abstract>.
- [20] Zanariah Hashim, Yukio Mukai, Takeshi Bamba, and Eiichiro Fukusaki. Metabolic profiling of retrograde pathway transcription factors *rtg1* and *rtg3* knockout yeast. *Metabolites*, 4(3):580–98, 2014. ISSN 2218-1989. doi: 10.3390/metabo4030580. URL <http://www.mdpi.com/2218-1989/4/3/580/htm>.
- [21] Beverly A. Rothermel, Janet L. Thornton, and Ronald A. Butow. *Rtg3p*, a basic helix-loop-helix/leucine zipper protein that functions in mitochondrial-induced changes in gene expression, contains independent activation domains. *Journal of Biological Chemistry*, 272(32):19801–19807, 8 1997. ISSN 00219258. doi: 10.1074/jbc.272.32.19801.
- [22] Thomas M. Cover and Joy A. Thomas. *Elements of Information Theory*. Wiley, 9 2005. ISBN 9780471241959. doi: 10.1002/047174882X. URL <https://onlinelibrary.wiley.com/doi/book/10.1002/047174882X>.
- [23] Josh H McDermott. The cocktail party problem. *Current Biology*, 19(22):R1024–R1027, 2009.
- [24] D Jouan-Rimbaud Bouveresse and DN Rutledge. Independent components analysis:

theory and applications. In *Data Handling in Science and Technology*, volume 30, pages 225–277. Elsevier, 2016.



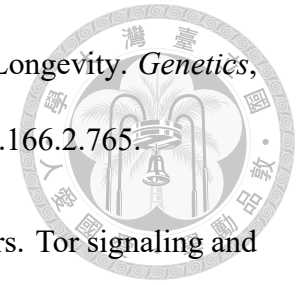
- [25] TA Trendeleva and RA Zvyagilskaya. Retrograde signaling as a mechanism of yeast adaptation to unfavorable factors. *Biochemistry (Moscow)*, 83(2):98–106, 2018. doi: 10.1134/S0006297918020025.
- [26] Zeeshan Fatima, Bablu Kumar, Suriya Rehman, and Saif Hameed. Retrograde signaling: A novel antifungal drug target. In *New and Future Developments in Microbial Biotechnology and Bioengineering*, pages 219–226. Elsevier, 2020. doi: 10.1016/B978-0-12-820528-0.00015-6. URL <https://linkinghub.elsevier.com/retrieve/pii/B9780128205280000156>.
- [27] Zhengchang Liu, Takayuki Sekito, Charles B. Epstein, and Ronald A. Butow. RTG-dependent mitochondria to nucleus signaling is negatively regulated by the seven WD-repeat protein Lst8p. *EMBO Journal*, 20(24):7209–7219, 2002. ISSN 02614189. doi: 10.1093/emboj/20.24.7209.
- [28] W. S. Moye-Rowley. Retrograde regulation of multidrug resistance in *Saccharomyces cerevisiae*. In *Gene*, volume 354, pages 15–21. Gene, 7 2005. doi: 10.1016/j.gene.2005.03.019. URL <https://pubmed.ncbi.nlm.nih.gov/15896930/>.
- [29] S. Hans, Z. Fatima, and S. Hameed. Retrograde signaling disruption influences ABC superfamily transporter, ergosterol and chitin levels along with biofilm formation in *Candida albicans*. *Journal de Mycologie Medicale*, 29(3):210–218, 9 2019. ISSN 17730449. doi: 10.1016/j.mycmed.2019.07.003.
- [30] Hongbo Yan, Yunying Zhao, and Linghuo Jiang. The putative transcription factor CaRtg3 is involved in tolerance to cations and antifungal drugs as well as serum-

induced filamentation in *Candida albicans*. *FEMS yeast research*, 14(4):614–623, 2014. doi: 10.1371/journal.pone.0203079.



- [31] S. Michal Jazwinski. The retrograde response: When mitochondrial quality control is not enough. *Biochimica et Biophysica Acta - Molecular Cell Research*, 1833(2): 400–409, 2013. ISSN 01674889. doi: 10.1016/j.bbamcr.2012.02.010. URL <http://dx.doi.org/10.1016/j.bbamcr.2012.02.010>.
- [32] Brian P. Ingalls. *Mathematical Modelling in Systems Biology : An Introduction*, volume 53. 2013. ISBN 978-0-262-01888-3. doi: 10.1007/s00292-008-1023-1.
- [33] J J W Chen, K Peck, T M Hong, S C Yang, Y P Sher, J Y Shih, R Wu, J L Cheng, S R Roffler, C W Wu, and P C Yang. Global analysis of gene expression in invasion by a lung cancer model. *Cancer Research*, 61:5223–5230, 2001. ISSN 0008-5472.
- [34] Mercè Gomar-Alba, Ma Angeles Morcillo-Parra, and Marcel Li Del Olmo. Response of yeast cells to high glucose involves molecular and physiological differences when compared to other osmostress conditions. *FEMS Yeast Research*, 15(5):fov039, aug 2015. doi: 10.1093/femsyr/fov039. URL <http://dx.doi.org/10.1093/femsyr/fov039>.
- [35] Nan Hao, Bogdan A. Budnik, Jeremy Gunawardena, and Erin K. O’Shea. Tunable signal processing through modular control of transcription factor translocation. *Science*, 339(6118):460–464, 2013. ISSN 10959203. doi: 10.1126/science.1227299.
- [36] Christopher Rackauckas and Qing Nie. Differentialequations.jl – a performant and feature-rich ecosystem for solving differential equations in julia. *Journal of open research software*, 5, May 2017. doi: 10.5334/jors.151.
- [37] Corina Borghouts, Alberto Benguria, Jaroslaw Wawryn, and S. Michal Jazwinski.

Rtg2 Protein Links Metabolism and Genome Stability in Yeast Longevity. *Genetics*, 166(2):765–777, 2004. ISSN 00166731. doi: 10.1534/genetics.166.2.765.



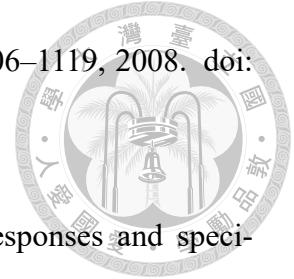
- [38] Ivanka Dilova, Sofia Aronova, Jenny C Y Chen, and Ted Powers. Tor signaling and nutrient-based signals converge on Mks1p phosphorylation to regulate expression of Rtg1p Rtg3p-dependent target genes. *Journal of Biological Chemistry*, 279(45): 46527–46535, 2004. ISSN 00219258. doi: 10.1074/jbc.M409012200.
- [39] José Ribamar Ferreira Júnior, Mário Spírek, Zhengchang Liu, and Ronald A Butow. Interaction between rtg2p and mks1p in the regulation of the RTG pathway of *Saccharomyces cerevisiae*. *Gene*, 354:2–8, jul 2005. doi: 10.1016/j.gene.2005.03.048. URL <http://dx.doi.org/10.1016/j.gene.2005.03.048>.
- [40] Rafaela Maria Rios-anjos, Vittoria De Lima Camandona, Lucas Bleicher, and Jose Ribamar Ferreira-junior. Structural and functional mapping of Rtg2p determinants involved in retrograde signaling and aging of *Saccharomyces cerevisiae*. pages 1–27, 2017. ISSN 1932-6203. doi: 10.1371/journal.pone.0177090.
- [41] José Ribamar Ferreira, Mário Spírek, Zhengchang Liu, and Ronald A. Butow. Interaction between Rtg2p and Mks1p in the regulation of the RTG pathway of *Saccharomyces cerevisiae*. *Gene*, 354(1-2 SPEC. ISS.):2–8, 2005. ISSN 03781119. doi: 10.1016/j.gene.2005.03.048.
- [42] Stefan Legewie, Nils Blüthgen, and Hanspeter Herzl. Quantitative analysis of ultrasensitive responses. *FEBS Journal*, 272(16):4071–4079, 8 2005. ISSN 1742464X. doi: 10.1111/j.1742-4658.2005.04818.x. URL <http://doi.wiley.com/10.1111/j.1742-4658.2005.04818.x>.
- [43] James E Ferrell and Sang Hoon Ha. Ultrasensitivity part I: Michaelian responses and

zero-order ultrasensitivity, 2014. ISSN 13624326. URL <http://dx.doi.org/10.1016/j.tibs.2014.08.003>.



- [44] Takayuki Sekito, Zhengchang Liu, Janet Thornton, and Ronald A. Butow. RTG-dependent mitochondria-to-nucleus signaling is regulated by MKS1 and is linked to formation of yeast prion [URE3]. *Molecular biology of the cell*, 13(3):795–804, 3 2002. ISSN 1059-1524. doi: 10.1091/mbc.01-09-0473.
- [45] Zhi Xin Wang. An exact mathematical expression for describing competitive binding of two different ligands to a protein molecule. *FEBS Letters*, 360(2):111–114, 2 1995. ISSN 00145793. doi: 10.1016/0014-5793(95)00062-E. URL <http://doi.wiley.com/10.1016/0014-5793%2895%2900062-E>.
- [46] Uri Alon. An introduction to systems biology: design principles of biological circuits. pages 37–54. CRC press, 2019. ISBN 978-1439837177. doi: 10.1201/9780429283321.
- [47] Pablo A Iglesias and Brian P Ingalls. Control theory and systems biology. chapter 10. MIT Press, 2009. ISBN 0262013347.
- [48] Daniel T Gillespie. Chemical Langevin equation. *Journal of Chemical Physics*, 113 (1):297–306, 2000. ISSN 00219606. doi: 10.1063/1.481811. URL <https://doi.org/10.1063/1.481811>.
- [49] Mukund Thattai and Alexander van Oudenaarden. Attenuation of noise in ultrasensitive signaling cascades. *Biophysical journal*, 82(6):2943–2950, 2002. doi: 10.1016/S0006-3495(02)75635-X.
- [50] Nicolas E Buchler and Matthieu Louis. Molecular titration and ultrasensitivity in

regulatory networks. *Journal of molecular biology*, 384(5):1106–1119, 2008. doi: 10.1016/j.jmb.2008.09.079.

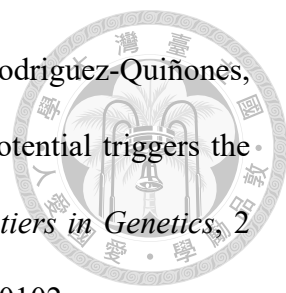


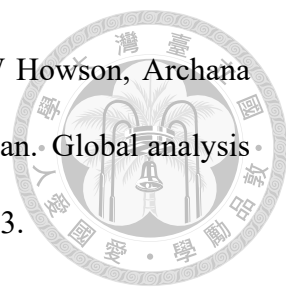
- [51] Seth Haney, Lee Bardwell, and Qing Nie. Ultrasensitive responses and specificity in cell signaling. *BMC systems biology*, 4(1):119, 2010. doi: 10.1186/1752-0509-4-119.
- [52] Lars Folke Olsen, Ann Zahle Andersen, Anita Lunding, Jens Christian Brasen, and Allan K Poulsen. Regulation of glycolytic oscillations by mitochondrial and plasma membrane h^+ -atpases. *Biophysical Journal*, 96(9):3850–3861, 2009. doi: 10.1016/j.bpj.2009.02.026.
- [53] Aidar D Satroutdinov, Hiroshi Kuriyama, and Harumi Kobayashi. Oscillatory metabolism of *Saccharomyces cerevisiae* in continuous culture. *FEMS microbiology letters*, 98(1-3):261–267, 1992. doi: 10.1111/j.1574-6968.1992.tb05525.x.
- [54] Peter Richard. The rhythm of yeast. *FEMS microbiology reviews*, 27(4):547–557, 2003. doi: 10.1016/S0168-6445(03)00065-2.
- [55] David Lloyd, L Eshantha, J Salgado, Michael P Turner, and Douglas B Murray. Respiratory oscillations in yeast: clock-driven mitochondrial cycles of energization. *FEBS letters*, 519(1-3):41–44, 2002.
- [56] David Lloyd, L Eshantha J Salgado, Michael P Turner, Marc TE Suller, and Douglas Murray. Cycles of mitochondrial energization driven by the ultradian clock in a continuous culture of *Saccharomyces cerevisiae*. *Microbiology*, 148(11):3715–3724, 2002.
- [57] David Lloyd, Katey M Lemar, L Eshantha J Salgado, Timothy M Gould, and Douglas B Murray. Respiratory oscillations in yeast: mitochondrial reactive oxygen

species, apoptosis and time; a hypothesis. *FEMS yeast research*, 3(4):333–339, 2003.
doi: 10.1016/S1567-1356(03)00071-0.



- [58] Douglas B Murray, Sibel Roller, Hiroshi Kuriyama, and David Lloyd. Clock control of ultradian respiratory oscillation found during yeast continuous culture. *Journal of Bacteriology*, 183(24):7253–7259, 2001. doi: 10.1128/JB.183.24.7253–7259.2001.
- [59] S. Adel Sedra and C. Kenneth Smith. Microelectronic circuits. chapter 9. 2009. ISBN 978-0195323030.
- [60] R a Butow. Cellular responses to mitochondrial dysfunction: it's not always downhill. *Cell death and differentiation*, 9(10):1043–5, 2002. ISSN 1350-9047. doi: 10.1038/sj.cdd.4401083. URL <http://www.ncbi.nlm.nih.gov/pubmed/12232791>.
- [61] Sean P. Whelan and Brian S. Zuckerbraun. Mitochondrial signaling: Forwards, backwards, and in between. *Oxidative Medicine and Cellular Longevity*, 2013:1–10, 2013. ISSN 1942-0900. doi: 10.1155/2013/351613.
- [62] Emma Heart, Gordon C Yaney, Richard F Corkey, Vera Schultz, Esthere Luc, Lihan Liu, Jude T Deeney, Orian Shirihai, Keith Tornheim, Peter JS Smith, et al. Ca^{2+} , nad (p) h and membrane potential changes in pancreatic β -cells by methyl succinate: comparison with glucose. *Biochemical Journal*, 403(1):197–205, 2007. doi: 10.1042/BJ20061209.
- [63] Walter W. Chen, Elizaveta Freinkman, Tim Wang, K??van?? Birsoy, and David M. Sabatini. Absolute Quantification of Matrix Metabolites Reveals the Dynamics of Mitochondrial Metabolism. *Cell*, 2016. ISSN 10974172. doi: 10.1016/j.cell.2016.07.040.

- 
- [64] Michael V. Miceli, James C. Jiang, Anurag Tiwari, Jose F. Rodriguez-Quinones, and S. Michal Jazwinski. Loss of mitochondrial membrane potential triggers the retrograde response extending yeast replicative lifespan. *Frontiers in Genetics*, 2 (JAN):1–11, 2012. ISSN 16648021. doi: 10.3389/fgene.2011.00102.
- [65] Thomas Nyström. Aging: Filtering out bad mitochondria. *Current Biology*, 23(23): 1037–1039, 2013. ISSN 09609822. doi: 10.1016/j.cub.2013.10.049.
- [66] Brooke E. Christian and Gerald S. Shadel. Aging: It's SIRTainly possible to restore mitochondrial dysfunction. *Current Biology*, 24(5):R206–R208, 2014. ISSN 09609822. doi: 10.1016/j.cub.2014.01.027. URL <http://dx.doi.org/10.1016/j.cub.2014.01.027>.
- [67] Parisa Badiie and Zahra Hashemizadeh. Opportunistic invasive fungal infections: diagnosis & clinical management. *The Indian journal of medical research*, 139(2): 195, 2014.
- [68] Kamila Jastrzebowska and Iwona Gabriel. Inhibitors of amino acids biosynthesis as antifungal agents. *Amino acids*, 47(2):227–249, 2015. doi: 10.1007/s00726-014-1873-1.
- [69] Mary T Pasko, Stephen C Piscitelli, and Andrea D Van Slooten. Fluconazole: a new triazole antifungal agent. *Dicp*, 24(9):860–867, 1990.
- [70] Shweta Singh, Zeeshan Fatima, Kamal Ahmad, and Saif Hameed. Fungicidal action of geraniol against candida albicans is potentiated by abrogated cacdr1p drug efflux and fluconazole synergism. *PloS one*, 13(8):e0203079, 2018. doi: 10.1371/journal.pone.0203079.

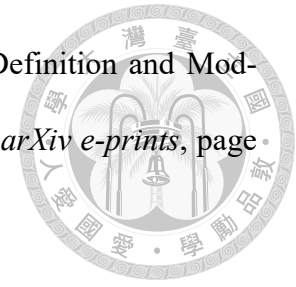
- 
- [71] Sina Ghaemmaghami, Won-Ki Huh, Kiowa Bower, Russell W Howson, Archana Belle, Noah Dephoure, Erin K O'Shea, and Jonathan S Weissman. Global analysis of protein expression in yeast. *Nature*, 425(6959):737–741, 2003.
- [72] Guido Van Rossum and Fred L. Drake. *Python 3 Reference Manual*. CreateSpace, Scotts Valley, CA, 2009. ISBN 1441412697.
- [73] John D Hunter. Matplotlib: A 2d graphics environment. *Computing in science & engineering*, 9(3):90–95, 2007.
- [74] Pauli Virtanen, Ralf Gommers, Travis E. Oliphant, Matt Haberland, Tyler Reddy, David Cournapeau, Evgeni Burovski, Pearu Peterson, Warren Weckesser, Jonathan Bright, Stéfan J. van der Walt, Matthew Brett, Joshua Wilson, K. Jarrod Millman, Nikolay Mayorov, Andrew R. J. Nelson, Eric Jones, Robert Kern, Eric Larson, C J Carey, İlhan Polat, Yu Feng, Eric W. Moore, Jake VanderPlas, Denis Laxalde, Josef Perktold, Robert Cimrman, Ian Henriksen, E. A. Quintero, Charles R. Harris, Anne M. Archibald, Antônio H. Ribeiro, Fabian Pedregosa, Paul van Mulbregt, and SciPy 1.0 Contributors. SciPy 1.0: Fundamental Algorithms for Scientific Computing in Python. *Nature Methods*, 17:261–272, 2020. doi: 10.1038/s41592-019-0686-2.
- [75] Charles R. Harris, K. Jarrod Millman, Stéfan J van der Walt, Ralf Gommers, Pauli Virtanen, David Cournapeau, Eric Wieser, Julian Taylor, Sebastian Berg, Nathaniel J. Smith, Robert Kern, Matti Picus, Stephan Hoyer, Marten H. van Kerkwijk, Matthew Brett, Allan Haldane, Jaime Fernández del Río, Mark Wiebe, Pearu Peterson, Pierre Gérard-Marchant, Kevin Sheppard, Tyler Reddy, Warren Weckesser, Hameer Abbasi, Christoph Gohlke, and Travis E. Oliphant. Ar-

ray programming with NumPy. *Nature*, 585:357 – 362, 2020. doi: 10.1038/s41586-020-2649-2.



- [76] Aaron Meurer, Christopher P Smith, Mateusz Paprocki, Ondřej Čertík, Sergey B Kirpichev, Matthew Rocklin, AMiT Kumar, Sergiu Ivanov, Jason K Moore, Sartaj Singh, et al. Sympy: symbolic computing in python. *PeerJ Computer Science*, 3: e103, 2017.
- [77] Takafumi Arakaki, Jake Bolewski, Robin Deits, Keno Fischer, Steven G. Johnson, Matthias Bussonnier, Isaiah Norton, Páll Haraldsson, Matthew Rocklin, Tsur, Viral B. Shah, Daniel Soto, eslgastal, Elias Kuthe, jakirkham, Marius Millea, grahamgill, fnmdx111, Alex Arslan, Darren Christopher Lukas, David Nadlinger, Lilian Besson, Sheehan Olver, Taine Zhao, and scls19fr. Juliapy/pyjulia: Pyjulia v0.5.6, November 2020. URL <https://doi.org/10.5281/zenodo.4294940>.
- [78] Wes McKinney. Data structures for statistical computing in python. In Stéfan van der Walt and Jarrod Millman, editors, *Proceedings of the 9th Python in Science Conference*, pages 51 – 56, 2010.
- [79] Mihails Delmans and Martin Hemberg. Discrete distributional differential expression (D3E) - a tool for gene expression analysis of single-cell RNA-seq data. *BMC Bioinformatics*, 17(1):110, 12 2016. ISSN 1471-2105. doi: 10.1186/s12859-016-0944-6. URL <http://www.biomedcentral.com/1471-2105/17/110>.
- [80] Jeff Bezanson, Alan Edelman, Stefan Karpinski, and Viral B Shah. Julia: A fresh approach to numerical computing. *SIAM review*, 59(1):65–98, 2017. URL <https://doi.org/10.1137/141000671>.
- [81] Mathieu Besançon, David Anthoff, Alex Arslan, Simon Byrne, Dahua Lin,

Theodore Papamarkou, and John Pearson. Distributions.jl: Definition and Modeling of Probability Distributions in the JuliaStats Ecosystem. *arXiv e-prints*, page arXiv:1907.08611, 7 2019.




- [82] John Myles White, Bogumił Kamiński, powerdistribution, Milan Bouchet-Valat, Sean Garborg, Jacob Quinn, Simon Kornblith, cjpriybol, Alexey Stukalov, Douglas Bates, Tom Short, Chris DuBois, Harlan Harris, Kevin Squire, Alex Arslan, pdeffebach, David Anthoff, Dave Kleinschmidt, Andreas Noack, Viral B. Shah, Alex Mellnik, Takafumi Arakaki, Tanmay Mohapatra, Peter, Stefan Karpinski, Dahua Lin, timema, ExpandingMan, Florian Oswald, and Lyndon White. Julia-data/dataframes.jl: v0.22.1, November 2020. URL <https://doi.org/10.5281/zenodo.4282946>.
- [83] James J Cai. scGEAToolbox: a matlab toolbox for single-cell RNA sequencing data analysis. *Bioinformatics*, nov 2019. doi: 10.1093/bioinformatics/btz830. URL <http://dx.doi.org/10.1093/bioinformatics/btz830>.
- [84] Christopher A Jackson, Dayanne M Castro, Giuseppe-Antonio Saldi, Richard Bonneau, and David Gresham. Gene regulatory network reconstruction using single-cell rna sequencing of barcoded genotypes in diverse environments. *Elife*, 9:e51254, 2020.
- [85] Jeff Bezanson, Stefan Karpinski, Viral B Shah, and Alan Edelman. Julia: A fast dynamic language for technical computing. *arXiv preprint arXiv:1209.5145*, 2012.
- [86] Jeffrey M Perkel. Julia: come for the syntax, stay for the speed. *Nature*, 572(7768): 141–143, 2019.



Appendix A — Key Resources

Deposited Data	REFERENCE	IDENTIFIER
RTG Microarray Data	[34]	GEO: GSE59569
RTG Microscopic Data	[14] and [44]	https://pubmed.ncbi.nlm.nih.gov/10848632/
Yeast GFP Database and Quantitative Western Blot	[71]	https://yeastgfp.yeastgenome.org/
Software and algorithms		
Python (v3.7)	[72]	https://www.python.org/
Matplotlib (v3.1.1)	[73]	https://matplotlib.org/
Scipy	[74]	https://www.scipy.org/
Numpy (v1.19.0)	[75]	https://numpy.org/
Sympy (v1.6)	[76]	https://www.sympy.org/
PyJulia (v0.5.6)	[77]	https://github.com/JuliaPy/pyjulia
Pandas (v1.0.5)	[78]	https://pandas.pydata.org/



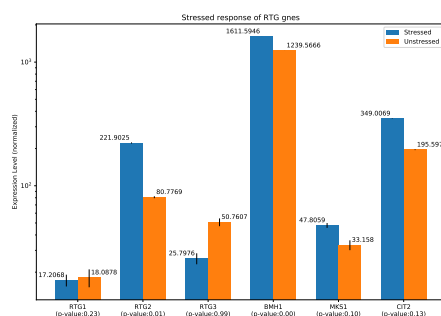
D ³ E: : Discrete Distributional Differential Expression	[79]	https://github.com/hemberg-lab/D3E
Julia (v1.5.3)	[80]	https://julialang.org/
DifferentialEquations.jl (v6.15.0)	[36]	https://github.com/SciML/DifferentialEquations.jl
Dierckx.jl (v0.5.0)	N/A	https://github.com/kbarbary/Dierckx.jl
Distributions.jl (v0.23.8)	[81]	https://doi.org/10.5281/zenodo.2647458
DataFrames.jl (v0.22.1)	[82]	https://github.com/JuliaData/DataFrames.jl
FindSteadyStates.jl (v0.1.1)	This paper	https://github.com/stevengogogo/FindSteadyStates.jl
EstimHill.jl (v0.1.0)	This paper	https://github.com/stevengogogo/EstimHill.jl
PotentialMap.jl (v0.1.0)	This paper	https://github.com/stevengogogo/PotentialMap.jl

Table A.1. Key Resources

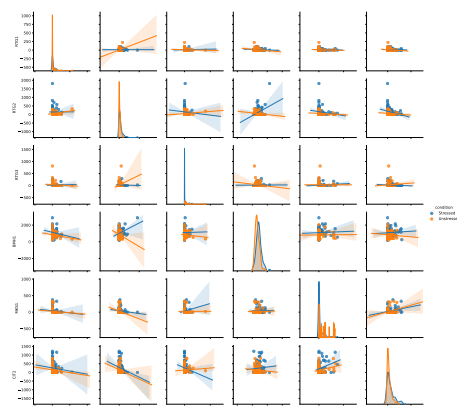


Appendix B — Boolean model of mitochondrial retrograde signaling

B.0.4 Stress response and expression levels



(a) Expression Level of Retrograde Proteins



(b) Correlation of each RTG genes in response to stress

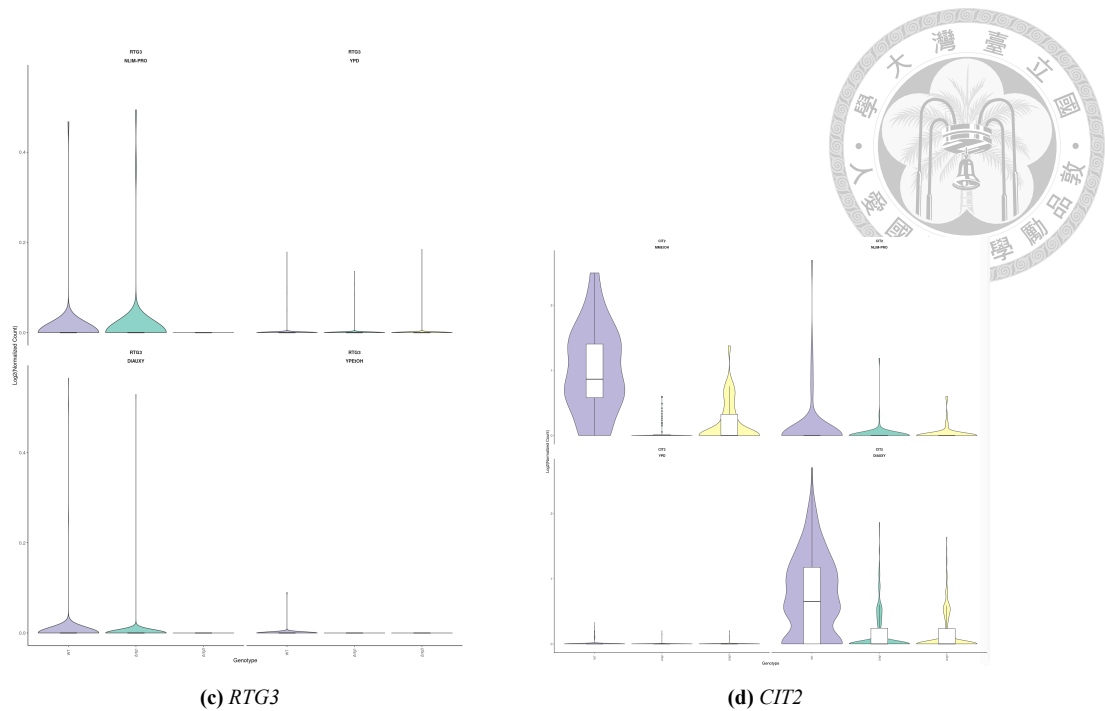


Figure B.1. Expression levels of RTG proteins. (a,b) Comparative expressions between retrograde signaling genes under osmotic stress. The microarray data were taken from the Gene Expression Omnibus(GEO) database (access number GSE59569)[34] (c,d) Violin plots of the \log_2 batch-normalized expression of the general retrograde gene *RTG3* and *CIT2* in YPD, DIAUXY (diauxic shift), MMETOH (minimum medium), and NLIM-PRO (proline-limited media).

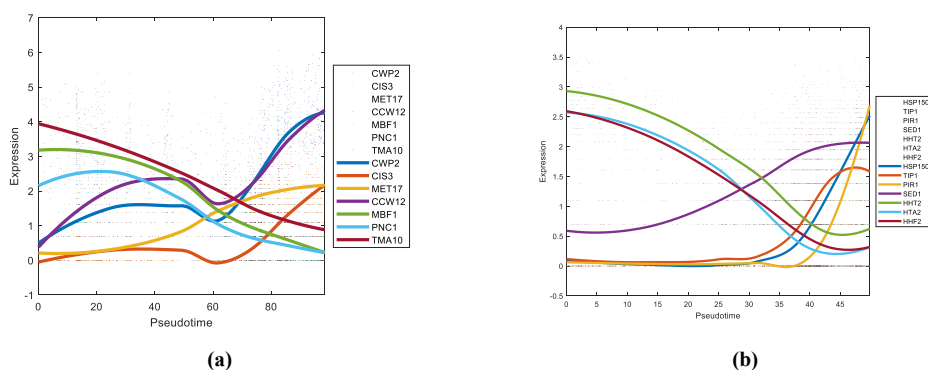


Figure B.2. Pseudo time plots of yeast gene expression. By using single-cell RNAseq bioinformatic toolbox scGEAToolbox[83], the single-cell RNAseq data were taken from the GEO database(accession number GSE125162)[84].

B.0.5 Model with dynamical inputs

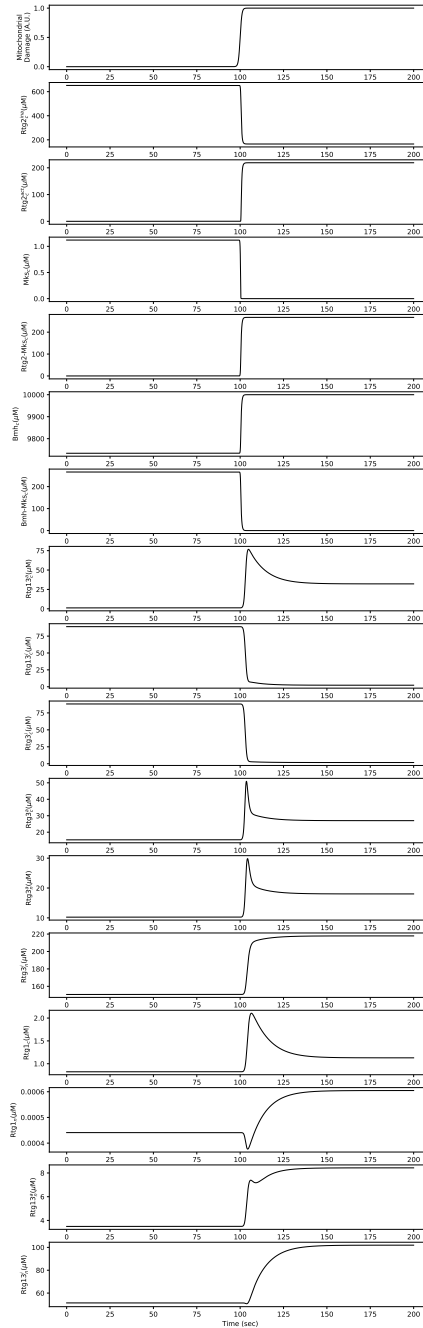
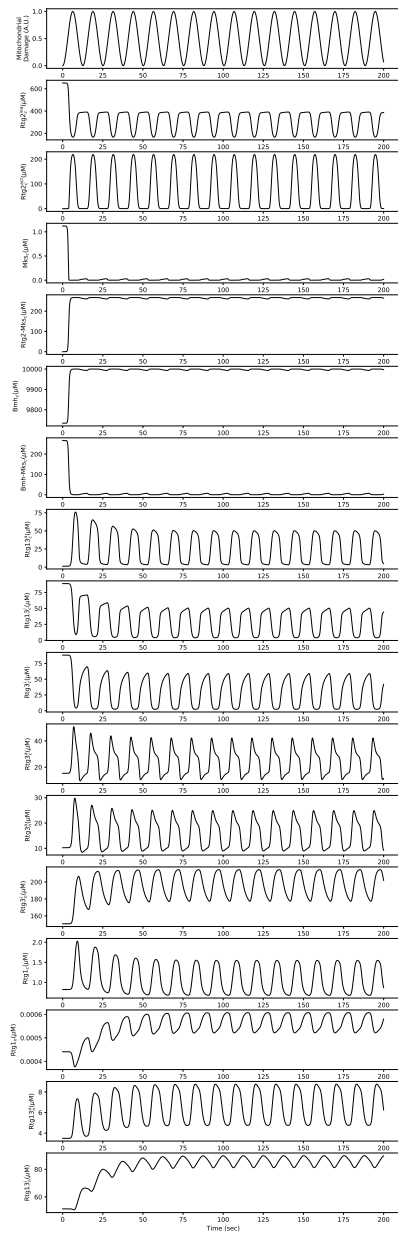
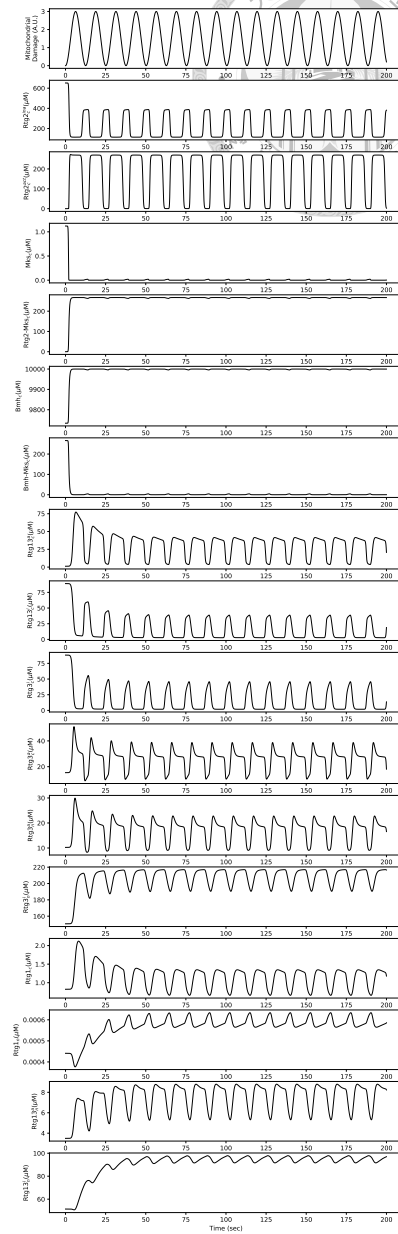


Figure B.3. The retrograde response to mitochondrial damage with sigmoid. The step response. When applying sharp sigmoid signal, there is overshoot effect on $Rtg3p_c^a$, $Rtg3p_n^a$, $Rtg1p_c$, $Rtg1p_c$ and $Rtg1p_n^a$.

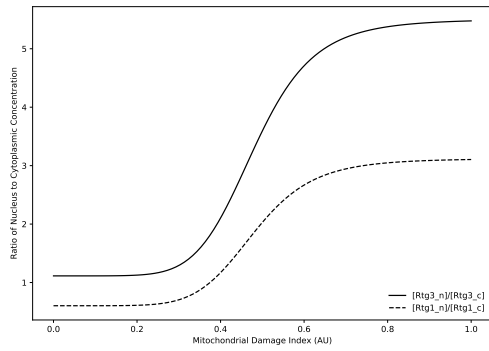


(a)

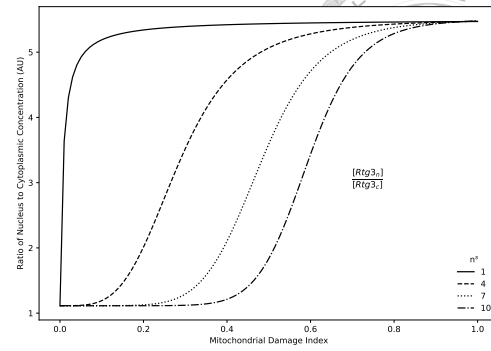


(b)

Figure B.3. The retrograde response to mitochondrial damage with square and sinusoidal waveforms. Both waveforms have similar characteristics: The inactive form of \neg Rtg3p performs with impulse train and Rtg1/3p_n^a with the square wave containing overshoot when the step changing as ON. The Mks associated components remains nearly steady with small ripples responding to the periodic input signal.



(a)



(b)

Figure B.4. The input-output relation and Hill coefficient. (a) The influence of Hill coefficient of input sensing (n_s) on nucleus accumulation. The Rtg2p sensing of mitochondrial damage signal is modelled by the Hill equation with the parameter of Hill coefficient, n^s . It is still unclear the mechanism of Rtg2p activation induced by mitochondrial damage. Therefore, the Hill equation is used to generalize the reaction. In our model, when the Hill coefficient equals to 1. The nucleus accumulation is rigidly responding to the mitochondrial damage signal. However, when Hill coefficient is greater than 1, the curve of phase plot becomes steady but gradually increasing the threshold. (b) The phase plot of Nucleus accumulation responding to mitochondrial damage signal. The nucleus accumulation is measured by dividing the nucleus total concentration by the cytoplasmic total concentration. Both Rtg1p and Rtg3p accumulates to nucleus with a monotonous trend when the the mitochondrial damage signal high.

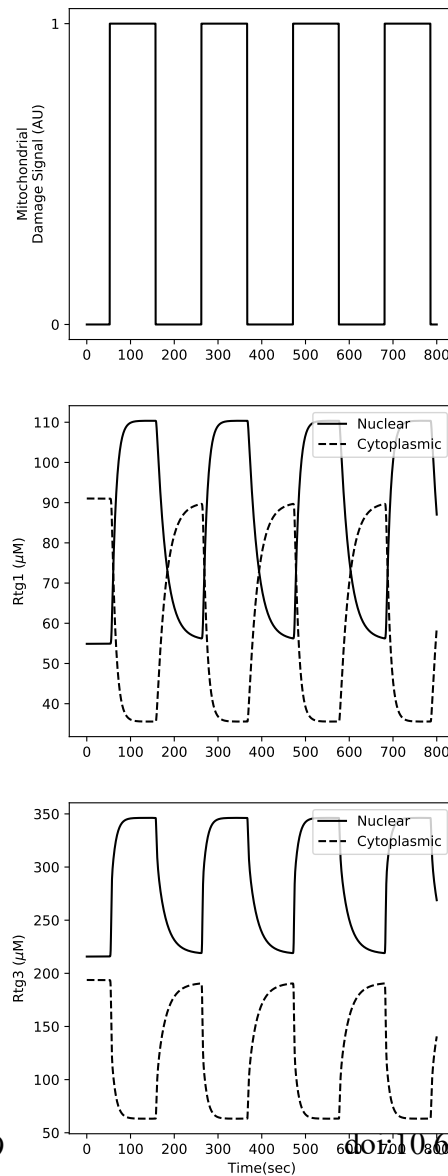
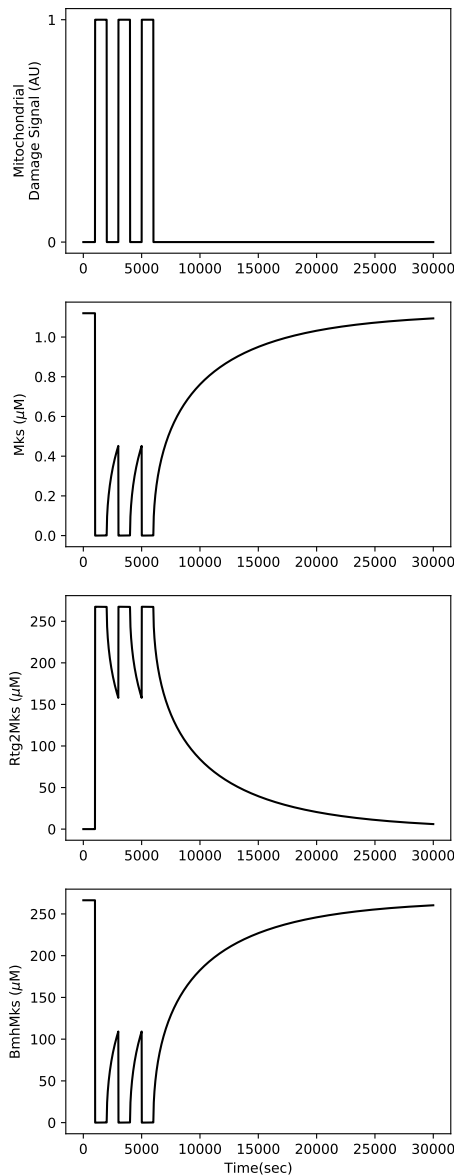


Figure B.5. The square wave response of the proposed mitochondrial retrograde signalling model. (a) The square wave response of Mksp and its heterodimers, Bmh/Mksp and Rtg2mksp, reveals the sign-sensitive delay pattern, where the delay depends on the sign of the step, ON or OFF. Mksp The sign-sensitive delay can protect against input fluctuations. The high binding coefficient of Mksp and its partners, Bmhp and Rtg2p, results in low concentration of unbinding Mks. (b) Steady-state abundance of Rtg1/3p in nucleus and cytosol in response to the mitochondrial damage. The Nuclear accumulation of Rtg1p and Rtg3p induced by mitochondrial damage with square wave signal. Unlike Mksp, The delay of square response of Rtg1/Rtg3p is insensitive to the sign of the step. The Rtg1p and Rtg3p accumulate to nucleus when the damage signal turns ON. Noted that the nuclear concentration of Rtg3p is always higher than the cytoplasmic one whenever mitochondrial damage signal is ON or OFF [27].

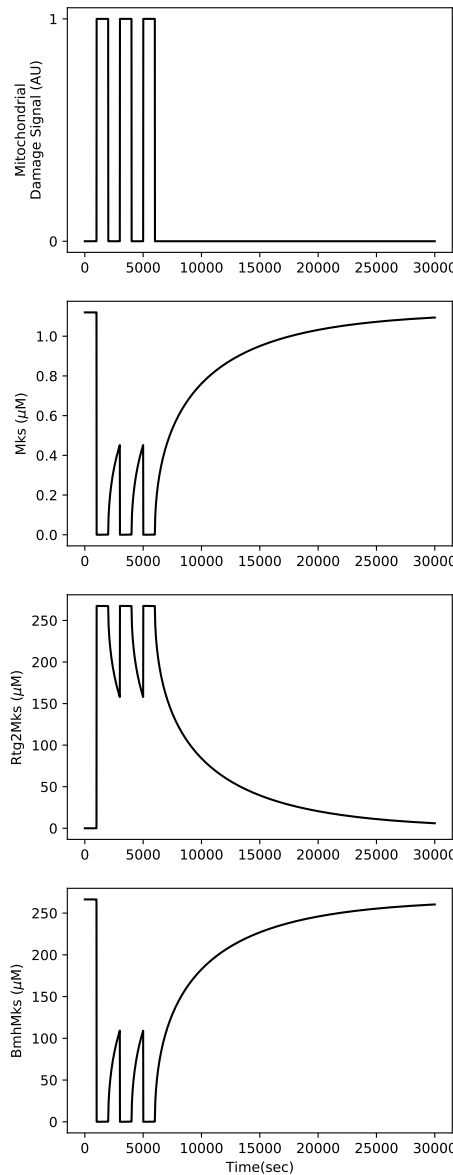


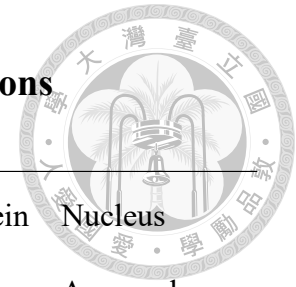
Figure B.6. The steady-state of Mksp and its heterodimers. After inducing by the mitochondrial damage signal, The ON state of RTG network slowly shuts down after inducing a short period of stimulation.



Table of RTG-associated Proteins[17, 14, 40]			
Standard Name	Systematic Codes	Function	Human homolog
Rtg1 / Rtg3	YOL067C / YBL103C	Activates retrograde response	MYC-MAX
Rtg2	YGL252C	Promotes translocation of Rtg1-Rtg3 from cytosol to nucleus; binds with Mks1	unclear[17]
Mks1	YNL076W	Phospholates Rtg3; downregulates RTG pathway	MKS1
Bmh1	YER177W	Binds with Mks1, and forms Bmh1/2-Mks1 to phosphate Rtg3	YWHAE

Table B.2. RTG-associated proteins. This table contains proteins which are associated with yeast mitochondrial retrograde response, and human homologs are also referenced.

B.0.6 Rtg1/3p Translocation under Multple Conditions



Rtg1p	Rtg2p	Rtg3p	Mito-damage	Mks	GFP-labelled protein	Nucleus Accumula- tion[14, 44]
0	0	1	0	1	Rtg3-GFP	N/A
0	0	1	1	1	Rtg3-GFP	1
0	1	1	0	1	Rtg3-GFP	1
0	1	1	1	1	Rtg3-GFP	1
1	0	1	0	1	Rtg3-GFP	0
1	0	1	1	1	Rtg3-GFP	0
1	1	1	0	1	Rtg3-GFP	0
1	1	1	1	1	Rtg3-GFP	1
1	0	0	0	1	Rtg1-GFP	N/A
1	0	0	1	1	Rtg1-GFP	N/A
1	1	0	0	1	Rtg1-GFP	0
1	1	0	1	1	Rtg1-GFP	0
1	0	1	0	1	Rtg1-GFP	0
1	0	1	1	1	Rtg1-GFP	0
1	1	1	0	1	Rtg1-GFP	0
1	1	1	1	1	Rtg1-GFP	1
1	0	1	0	0	Rtg3-GFP	1
1	1	1	0	0	Rtg3-GFP	1
1	0	1	0	0	Rtg1-GFP	1

1 1 1 0 0 Rtg1-GFP



Table B.4. The qualitative input-output relations of retrograde response. The translocation and phosphorylation state of Rtg3p is determined by the functional state of mitochondria. When *CIT2* expression is low, which means the retrograde response is off, the transcription factor Rtg3p is localized mainly in the cytoplasm and multiply phosphorylated [14]). When Rtg3p locates in the nucleus in ρ_0 cells, Rtg3p is partially dephosphorylated, and the nuclear localization sequence on Rtg3p results in its nucleus accumulation. Though the expression of *CIT2* requires both Rtg3p and Rtg1p, the phosphorylation state of Rtg1p between wild type and ρ_0 cells has no detectable difference. Rtg1p may be anchored by the nucleus via [14]. The existence of RTG proteins and mitochondrial damage signal is described in binary quantity. The 0 represents the deleted protein or absence of mitochondrial damage, and 1 vice versa. Untested conditions are labelled with N/A.

Mitochondrial Damage Signal	Existence of Rtg3p	Existence of Rtg2p	Nucleus Accumulation of Rtg1p[14]
> 0	> 0	= 0	No
> 0	= 0	= 0	No
> 0	= 0	> 0	No
= 0	> 0	> 0	Yes
= 0	> 0	= 0	Yes
= 0	> 0	> 0	Yes
= 0	= 0	= 0	Yes
= 0	= 0	> 0	Yes

a Translocation of Rtg1-GFP

Mitochondrial Damage Signal	Existence of Rtg1p	Existence of Rtg2p	Nucleus Accumulation of Rtg3p[14]
> 0	> 0	= 0	No
> 0	= 0	= 0	Yes
> 0	= 0	> 0	Yes
= 0	> 0	= 0	No
= 0	> 0	> 0	No
> 0	> 0	> 0	Yes

b Translocation of Rtg3-GFP

Mitochondrial Damage Signal	Existence of Mksp	Existence of Rtg2p	Nucleus Accumulation of Rtg1p and Rtg3p[44]
> 0	= 0	= 0	Yes
> 0	= 0	> 0	Yes

c Translocation of Rtg1-GFP and Rtg3-GFP in Δmks .

Table B.5. Properties of Rtg1/3p translocation to nucleus. Deleted proteins are presented with 0, and wild type protein are assumed to be greater than 0.

B.0.7 Ordinary differential equation-based model of mitochondrial retrograde signaling



Activation Layer

$$\frac{ds(t)}{dt} = 0 \quad (B.1)$$

$$\frac{dRtg2_c^i}{dt} = - \frac{k^{s_v} (s(t))^{n_s}}{k^{s_d n_s} + (s(t))^{n_s}} Rtg2_c^{ina}(t) + k_I^r Rtg2_c^{act}(t) \quad (B.2)$$

$$\frac{dRtg2_{act_c}(t)}{dt} = \frac{k^{s_v} (s(t))^{n_s}}{k^{s_d n_s} + (s(t))^{n_s}} Rtg2_c^{ina}(t) \quad (B.3)$$

$$- k_I^r Rtg2_c^{act}(t) - k^{rm} Rtg2_c^{act}(t) Mks(t) + k_I^{rm} Rtg2Mks_c(t)$$

$$\frac{dMks(t)}{dt} = - k^{rm} Rtg2_c^{act}(t) Mks(t) + \quad (B.4)$$

$$k_I^{rm} Rtg2Mks_c(t) - k^{bm} Bmh(t) Mks(t) + k_I^{bm} BmhMks(t)$$

$$\frac{dRtg2Mks_c(t)}{dt} = k^{rm} Rtg2_c^{act}(t) Mks(t) - k_I^{rm} Rtg2Mks_c(t) \quad (B.5)$$

$$\frac{dBmh(t)}{dt} = - k^{bm} Bmh(t) Mks(t) + k_I^{bm} BmhMks(t) \quad (B.6)$$

$$\frac{dBmhMks(t)}{dt} = k^{bm} Bmh(t) Mks(t) \quad (B.7)$$

$$- k_I^{bm} BmhMks(t) \quad (B.8)$$

Modulation Layer

$$\frac{dRtg13_{a_c}(t)}{dt} = - \left(k_I^{13} + \frac{Rtg2_c^{ina} k_{vI}^{13} BmhMks(t)}{k_{ID}^{13} + BmhMks(t)} \right) Rtg13_c^a(t) \quad (B.9)$$

$$+ k_c^{13} Rtg1_c(t) Rtg3_c^a(t) - k_{cI}^{13} Rtg13_c^a(t) \quad (B.10)$$

$$\frac{dRtg13_{i_c}(t)}{dt} = \left(k_I^{13} + \frac{Rtg2_c^{2ina} k_{v_I}^{13} BmhMks(t)}{k_{ID}^{13} + BmhMks(t)} \right) Rtg13_c^a(t) \quad (B.11)$$

$$+ k_c^{13} Rtg1_c(t) Rtg3_c^i(t) - k_{c_I}^{13} Rtg13_c^i(t) \quad (B.12)$$

$$\begin{aligned} \frac{dRtg3_{i_c}(t)}{dt} = & -k_{c_A}^3 Rtg3_c^i(t) + k_{c_I}^3 Rtg3_c^a(t) \\ & - k_c^{13} Rtg1_c(t) Rtg3_c^i(t) + k_{c_I}^{13} Rtg13_c^i(t) \\ & - k_{i_{in}}^3 Rtg3_c^i(t) + k_{i_{out}}^3 Rtg3_n^i(t) \end{aligned}$$

$$\frac{dRtg3_{a_c}(t)}{dt} = k_{c_A}^3 Rtg3_c^i(t) - k_{c_I}^3 Rtg3_c^a(t) \quad (B.13)$$

$$\begin{aligned} & - k_c^{13} Rtg1_c(t) Rtg3_c^a(t) + k_{c_I}^{13} Rtg13_c^a(t) \\ & - k_{a_{in}}^3 Rtg3_c^a(t) + k_{a_{out}}^3 Rtg3_n^a(t) \end{aligned}$$

$$\frac{dRtg3_{a_n}(t)}{dt} = -k_{n_I}^3 Rtg3_n^a(t) - k_n^{13} Rtg1_n(t) Rtg3_n^a(t) \quad (B.14)$$

$$\begin{aligned} & + k_{n_I}^{13} Rtg13_n^a(t) + k_{a_{in}}^3 Rtg3_c^a(t) \\ & - k_{a_{out}}^3 Rtg3_n^a(t) \end{aligned}$$

$$\frac{dRtg3_{i_n}(t)}{dt} = k_{n_I}^3 Rtg3_n^a(t) - k_n^{13} Rtg1_n(t) Rtg3_n^i(t) \quad (B.15)$$

$$\begin{aligned} & + k_{n_I}^{13} Rtg13_n^i(t) + k_{i_{in}}^3 Rtg3_c^i(t) \\ & - k_{i_{out}}^3 Rtg3_n^i(t) \end{aligned}$$

$$\frac{dRtg1_{c}(t)}{dt} = -k_c^{13} Rtg1_c(t) Rtg3_c^a(t) \quad (B.16)$$

$$\begin{aligned} & + k_{c_I}^{13} Rtg13_c^a(t) - k_c^{13} Rtg1_c(t) Rtg3_c^i(t) \\ & + k_{c_I}^{13} Rtg13_c^i(t) \\ & - k_{in}^1 Rtg1_c(t) + k_{out}^1 Rtg1_n(t) \end{aligned}$$

$$\frac{dRtg1_{n}(t)}{dt} = -k_n^{13} Rtg1_n(t) Rtg3_n^a(t) \quad (B.17)$$

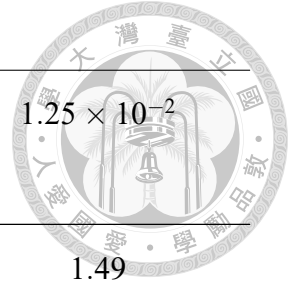
$$\begin{aligned} & + k_{n_I}^{13} Rtg13_n^a(t) - k_n^{13} Rtg1_n(t) Rtg3_n^i(t) \\ & + k_{n_I}^{13} Rtg13_n^i(t) + k_{in}^1 Rtg1_c(t) - k_{out}^1 Rtg1_n(t) \end{aligned}$$

$$\frac{dRtg13_{a_n}(t)}{dt} = k_n^{13} Rtg1_n(t) Rtg3_n^a(t) - k_{n_I}^{13} Rtg13_n^a(t) \quad (B.18)$$

$$\frac{dRtg13_{i_n}(t)}{dt} = k_n^{13} Rtg1_n(t) Rtg3_n^i(t) - k_{n_I}^{13} Rtg13_n^i(t) \quad (B.19)$$

B.0.8 Fitted parameters

Kinetic Coeff.	Description	Value (AU)
n_s	Hill coefficient of input signal	7
ksV	Maximum activation coefficient of Rtg2p	1.17×10^1
ksD	Dissociation constant of Rtg2p activation	9.65×10^{-1}
$k2I$	Inactivation coefficient of Rtg2p	4.95
$k2M$	Binding coefficient of active Rtg2p and Mks	1.60×10^3
$kn2M$	Degradation coefficient of Rtg2pMks heterodimer	4.25×10^{-2}
kBM	Binding coefficient of Bmhp and Mksp	5.90×10^{-2}
$knBM$	Degradation coefficient of BmhpMks heterodimer	2.41
$k13I$	Maximum inactivation rate on Rtg1pRtg3 heterodimer	9.23×10^{-2}
$k13IV$	Maximum rate of Rtg3p inactivation	2.48×10^3
$k13ID$	Dissociation constant of Rtg3p inactivation	2.51×10^1
$k3A_c$	Kinetic coefficient of Rtg3p activation in cytosol	3.07×10^1

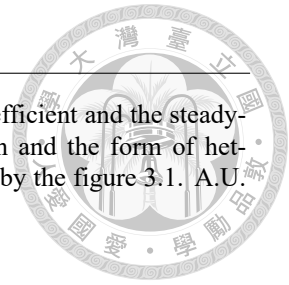


$k3I_c$	Kinetic coefficient of Rtg3p inactivation in cytosol	1.25×10^{-2}
$k3I_n$	Kinetic coefficient of Rtg3p inactivation in nucleus	1.49
$k13_c$	Kinetic coefficient of the binding of Rtg1p and Rtg3p in cytosol	2.34×10^2
$kn13_c$	Kinetic coefficient of Rtg1pRtg3 degradation in cytosol	2.21×10^2
$k13_n$	Kinetic coefficient of the binding of Rtg1p and Rtg3p in nucleus	4.61×10^2
$kn13_n$	Kinetic coefficient of Rtg1pRtg3 degradation in nucleus	5.96×10^{-1}
$k1in$	Kinetic coefficient of Rtg1p nucleus translocation from cytosol	3.20
$k1out$	Kinetic coefficient of Rtg1p cytoplasmic translocation from nucleus	5.97×10^3
$k3inA$	Kinetic coefficient of the nucleus translocation of active Rtg3p	1.02
$k3outA$	Kinetic coefficient of the cytoplasmic translocation of active Rtg3p	4.90×10^{-2}
$k3inI$	Kinetic coefficient of the nucleus translocation of inactive Rtg3p	3.80×10^{-2}



<i>k3outI</i>	Kinetic coefficient of the cytoplasmic translocation of inactive Rtg3p	1.23×10^{-1}
Protein	Concentration (AU)	
<i>Rtg2_c^{ina}</i>	Inactivated Rtg2p in cytosol	3.76×10^2
<i>Rtg2_c^{act}</i>	Activated Rtg3p in cytosol	8.78
<i>Mks</i>	Mksp protein (system name: Mks1p)	8.07×10^{-4}
<i>Rtg2Mks_c</i>	Heterodimer of Rtg2p and Mksp in cytosol	2.67×10^2
<i>Bmh</i>	Bmhp protein (including Bmh1p and Bmh2p)	10.00×10^3
<i>BmhMks</i>	Heterodimer of Bmhp and Mksp	1.97×10^{-1}
<i>Rtg13_c^{act}</i>	Heterodimer of Rtg1p and activated Rtg3p in cytosol	2.57×10^1
<i>Rtg13_c^{ina}</i>	Heterodimer of Rtg1p and inactivated Rtg3p in cytosol	2.14×10^1
<i>Rtg3_c^{ina}</i>	Inactivated Rtg3p in cytosol	1.71×10^1
<i>Rtg3_c^{act}</i>	Activated Rtg3p in cytosol	2.49×10^1
<i>Rtg3_n^{act}</i>	Activated Rtg3p in cytosol	1.66×10^1
<i>Rtg3_n^{ina}</i>	Inactivated Rtg3p in nucleus	2.06×10^2
<i>Rtg1_c</i>	Rtg1p in cytosol	1.06
<i>Rtg1_n</i>	Rtg1p in nucleus	5.67×10^{-4}
<i>Rtg13_n^{act}</i>	The heterodimer of Rtg1p and activated Rtg3p in nucleus	7.31
<i>Rtg13_n^{ina}</i>	The heterodimer of Rtg1p and inactivated Rtg3p in nucleus	9.04×10^1

Table B.6. Parameter set of the proposed model. The table includes the kinetic coefficient and the steady-state concentrations of RTG proteins categorized by the activation state, location and the form of heterodimer. The parameter fulfills the conditions listed in table B.4, and is validated by the figure 3.1. A.U. represents arbitrary unit.







Appendix C — Package development

The study of biological systems requires intense computational power to solve differential systems, Monte Carlo Simulation, parameter searching, and other quantitative analysis. Thus, delicately manipulating the computational resources is a way of harvesting the results. Low-level computer language like C/C++, which are interpretive languages, makes them suitable for creating fast and high efficient code compared to Python. However, writing these low-level languages is tedious and demanding for coding skills, and most prolonged the design process. On the contrary, Python is a high-level language with a simple syntax, providing lots of easy-to-use packages for writing simple and elegant code [72]. Because of its simplicity, Python has become a popular language for machine learning, scientific computing, and web design.

However, the curse of simplicity stems from its non-interpretive nature for machines, making Python code slow and inefficient. Though using Python can use callout commands optimized with C/Fortran wrapper, its simplicity makes it harder to manipulate the computation power like with low-level languages. This two-language dilemma limits the development of the software industry and scientific computing, including the field of computational biology.

The computation task of this study was first written in Python with *Scipy* and *Numpy*

packages, but the speed of *for-loop* in Python is slow, and the optimization with *Numba* package is limited. Later on, we transferred to Julia programming language to reach the high computational demands for solving biological systems and especially the parameter searching.

Julia is a new generic programming language aiming for scientific computing [85]. First released in 2012, making it a young language for this field. The key feature of Julia language is solving the two-language dilemma. Julia is a high-level language leveraged by multiple dispatch and metaprogramming, making the code simple as in Python. On the other hand, Julia is supported by the custom *LLVM* compiler, making it an interpretive language that can easily generate fast machine code and relatively easy to execute parallel processing with simple syntax [86].

By the aid of high performance computing with Julia, we have developed a workflow for building the mathematical model, parameter searching and system analysis. Moreover, the workflow was modularized into three packages for general usage (See Table. A.1): *FindSteadyStates.jl* for exploring the steady states of ordinary differential equations (ODE) with multi-threading; *EstimHill.jl* for sensitivity analysis with relative amplification approach and *PotentialMap.jl* for generating energy potential from ODE systems with Monte Carlo method and least action method.

The downside of using Julia programming language is the lack of packages due to its relatively small number of developers compared to popular languages like Python or R. In the following chapter, the developed package in this study will be introduced. We hope these packages developed in this study can further support the community.

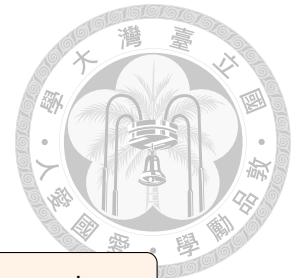
C.0.9 *FindSteadyStates.jl* - A Julia package for searching steady states of ODE systems



Finding steady states of ordinary differential equations (ODE) is essential for describing its systems behavior including robustness and stability. The steady state is the root solution of the system, which can be simply solved by matrix decomposition when the system is linear. However, finding roots of nonlinear equations is difficult, and most of the biological systems are nonlinear and even in high dimensions.

There are two methods for deriving the steady states: root finding algorithm and numerical simulation. The root finding algorithm finds the zeros of a continuous function based on iterative approach. On the other hand, the numerical simulation directly solve the ODE numerically until the variables reaches to a steady state. These two approaches require the initial guess of a steady state. To identify parameter sets, dense sampling within a domain is needed, which usually requires tremendous computational power and memory when the domain is broad.

Therefore, we created *FindSteadyStates.jl* to untangle the difficulty. This package combines the differential equation solver with the searching algorithm to find steady states in a given domain. This package provides two searching methods: random search and grid search in any given dimensionality. The grid search function is implemented in an iterator without consuming a vast of memory. Both search methods provide log scale sampling option with customizable exponential number. By the aid of *DifferentialEquations.jl* [36], this package can sampling a group of initial variables and dispatch them to multiple threads of CPUs (also known as multi-threading). In Figure C.7, the demonstration shows that how to use this package to derive the steady states of a bistable nonlinear model.



```

using FindSteadyStates
using DifferentialEquations

# Model
function bistable_ode!(du, u, p, t)
    s1, s2 = u
    K1, K2, k1, k2, k3, k4, n1, n2 = p
    du[1] = k1 / (1 + (s2/K2)^n1) - k3*s1
    du[2] = k2 / (1 + (s1/K1)^n2) - k4*s2
end

# Parameters
p_ = [1., 1., 20., 20., 5., 5., 4., 4.]
u_1 = [3., 1.]

# Define a problem
de = DEsteady(func=bistable_ode!,
              p=p_, u0=u_1,
              method=SSRootfind())

j_gen = jacobian(de) # jacobian generator

# Searching method and domain
param_gen = ParameterGrid([
    (0.1, 5., 100),
    (0.1, 5., 100)
])

# Solve
sols = solve(de, param_gen)

# Remove similar solutions
steadies = unique(sols)

# Jacobian
jac_ms = j_gen.(steadies)

# Stability
stab_modes = StabilityType.(jac_ms)

```

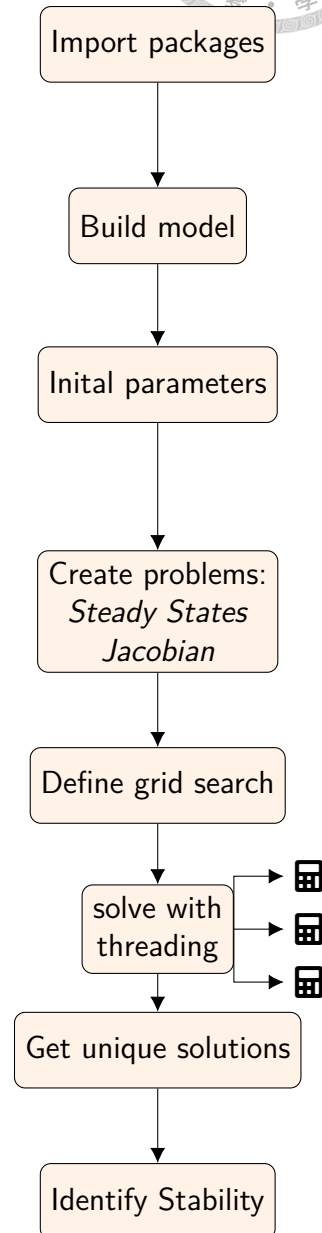


Figure C.7. Sample code for exploring steady states of an ODE model with *FindSteadyStates.jl*. A bistable model is defined with *bistable_ode!*. The parameters and initial guess of steady states is required to build the problem constructor - *de* and *j_gen* which generates steady states and jacobian. The domain of grid search is given in *ParameterGrid* command, and apply to the searching process with *solve* function which supports multi-threading for parallelization. Finally, use *unique* command to filter redundant solution set, and use the jacobian constructor (*j_gen*) to identify the stability of solutions.